Technical Report

TR-05-06

Galvanic corrosion of copper-cast iron couples

N R Smart, A P Rance and P A H Fennell
Serco Assurance

January 2005

Svensk Kärnbränslehantering AB
Swedish Nuclear Fuel
and Waste Management Co
Box 5864
SE-102 40 Stockholm Sweden
Tel 08-459 84 00
+46 8 459 84 00
Fax 08-661 57 19
+46 8 661 57 19

Galvanic corrosion of copper-cast iron couples

N R Smart, A P Rance and P A H Fennell
Serco Assurance

January 2005

Executive Summary

To ensure the safe encapsulation of spent nuclear fuel rods for geological disposal, SKB are considering using the Copper-Cast Iron Canister, which consists of an outer copper canister and an inner cast iron container. The canister will be placed into boreholes in the bedrock of a geologic repository and surrounded by bentonite clay. In the unlikely event of the outer copper canister being breached, water would enter the annulus between the inner and outer canister and at points of contact between the two metals there would be the possibility of galvanic interactions. Although this subject has been considered previously from both a theoretical standpoint and by experimental investigations there was a need for further experimental studies in support of information provided by SKB to the Swedish regulators (SKI).

In the work reported here copper-cast iron galvanic couples were set up in a number of different environments representing possible conditions in the SKB repository. The tests investigated two artificial porewaters at 30ºC and 50ºC, under aerated and deaerated conditions. Tests were also carried out in a 30 wt% bentonite slurry made up in artificial groundwater. The potential of the couples and the currents passing between the coupled electrodes were monitored for several months. The effect of growing an oxide film on the surface of the cast iron prior to coupling it with copper was investigated. In addition, some crevice specimens based on the multi-crevice assembly (MCA) design were used to simulate the situation where the copper canister will be in direct contact with the cast iron inner vessel.

The electrochemical results are presented graphically in the form of electrode potentials and galvanic corrosion currents as a function of time. The galvanic currents in aerated conditions were much higher than in deaerated conditions. For example, at 30ºC, galvanic corrosion rates as low as 0.02 µm/year for iron were observed after deaeration, but the corrosion rates were near 100 µm/year for the cast iron at 50ºC in the presence of oxygen. There was evidence of temporary polarity reversal at very low levels of current (i.e. the copper became the anode). The galvanic corrosion rates of iron coupled to copper at low groundwater oxygen concentrations were close to the values measured for anaerobic corrosion rates of uncoupled iron.

Under deaerated conditions a black film was formed on the surface of the cast iron, which was consistent with the formation of magnetite. The electrochemical potentials of the cast iron-copper couples in deaerated conditions were in the thermodynamically stable regions for magnetite and metallic copper.

The galvanic currents under deaerated conditions were higher at 50 ºC than at 30 ºC, by a factor of up to $\times 10$. This can be attributed to an increase in the exchange current density for the water reduction reaction on the copper cathode and to an increase in the rate of diffusion processes in the oxide film on cast iron.

There was some evidence for an increase in the galvanic corrosion rate in the presence of bentonite slurry compared to fully aqueous artificial groundwaters.

Pre-grown corrosion films on cast iron did not have a significant effect on subsequent measured galvanic corrosion rates when coupled to copper in deaerated conditions.

None of the MCA specimens exhibited any signs of galvanically enhanced crevice corrosion under deaerated conditions.

In terms of application of the results to the evolution of the environment within the annulus of the canister the following scenario is envisaged. If water penetrates the annulus through a hole in the outer copper container a galvanic couple will be set up between the copper and the cast iron insert. The current passing between the copper and the cast iron will be concentrated at the contact points. If any residual air is present in the annulus the corrosion rate of the cast iron will be enhanced (i.e. the

iron will be the anode and copper the cathode). In the absence of oxygen in the annulus, as a result of oxygen consumption by corrosion of the cast iron insert or by reaction with the surrounding matrix, the galvanic corrosion currents will fall markedly to values close to the corrosion rate of uncoupled cast iron.

Contents

Appendices

1 Introduction

To ensure the safe encapsulation of spent nuclear fuel rods for geological disposal, SKB are considering using the Copper- Cast Iron Canister, which consists of an outer copper canister and an inner cast iron container. The canister will be placed into boreholes in the bedrock of a geological repository and surrounded by bentonite clay. In the unlikely event of the outer copper canister being breached, water would enter the annulus between the inner and outer canister. At points of contact there would be the possibility of galvanic interactions between dissimilar metals, because there would be electronic contact between the copper and iron at the points where the inner and outer vessels touched and ionic contact with an electrolyte in the form of groundwater. The external pressure applied by the swelling bentonite would increase the number of electrical contact points between the inner and outer vessels. The rate of transport of both water and oxygen into the annulus would be restricted by the presence of the bentonite backfill.

In an early corrosion assessment of the canister design [1], the effects of an increase in the corrosion rate due to galvanic coupling between copper and steel were considered. Any possible increase in the hydrogen generation rate due to anaerobic corrosion of the iron was believed to be of relatively little importance, because it was assumed that hydrogen would expel the water from the annulus and the inner container would be in contact with the groundwater for a relatively short time.

Subsequently, a theoretical assessment of the risk of galvanic corrosion of copper-steel couples was carried out [2]. The main conclusions of the assessment were:

- In aerated conditions, coupling with copper would tend to increase the corrosion rate of the steel or cast iron. Corrosion of the carbon steel may be localised.

- The increase in corrosion rate of the steel would be limited by the slow diffusion of oxygen through the bentonite.

- Coupling in anoxic conditions would not be expected to increase the rate of gas generation due to the anaerobic corrosion of steel, because the rate of corrosion would be limited by the formation of a protective oxide film.

The effect of galvanically coupling copper with steel on the rate of gas generation due to anaerobic corrosion of the steel was investigated experimentally using the barometric gas cell technique [3]. The samples were produced by spot welding pieces of copper wire to pieces of carbon steel wire and the rate of gas generation was compared with that from a gas cell containing carbon steel only. It was found that there was no significant difference in the gas generation rate between the coupled and uncoupled specimens.

In order to confirm these predictions about the possible effects of galvanically coupling the cast iron and copper vessels and to address some of the issues raised in a report prepared for the Swedish regulator, SKI [4], some further experimental investigations of galvanic corrosion were conducted. The most commonly used methods for investigating galvanic interactions [5,6] between corroding metals are based on electrochemical techniques and in the work reported here these methods were applied to the SKB canister situation. A summary of the electrochemical theory describing galvanic corrosion, taken from reference [2], is reproduced in Appendix 1.

This report describes the measurements that were carried out to investigate the galvanic corrosion of copper-cast iron couples in anoxic conditions and applies the data to predicting the likely effect of galvanic corrosion on the performance of the canister design in the SKB repository.

2 Experimental

2.1 Overview of experimental programme

Uncoupled copper and cast iron electrodes and copper-cast iron couples were set up in a number of different environments simulating the environments expected in the SKB repository. The potentials of the electrodes and the currents passing between the coupled electrodes were monitored for a period of a few months. The differences between the electrochemical potentials of the uncoupled copper and cast iron electrodes indicate whether galvanic corrosion is likely and which electrode will corrode preferentially in the galvanic couple. Generally, it is found that the larger the separation in the electrochemical potentials the greater the severity of galvanic corrosion. The currents passing between the electrodes quantify the galvanic enhancement of the corrosion rate and show whether the corrosion rate changes with time; for example a decrease in the corrosion rate may occur as an oxide film develops on the surface of one of the electrodes. Current measurements also demonstrate whether there is any switching in polarity of the electrodes (i.e. whether the anode becomes the cathode or vice-versa).

In addition to the electrochemical measurements described above, the possibility of galvanically enhanced crevice corrosion was investigated using specimens composed of castellated cast iron nuts bolted tightly to copper sheet. These specimens were used to simulate the situation where the copper canister will be in direct contact with the inner cast iron vessel. The specimens were based on the multi-crevice assembly (MCA) design, which is commonly used for crevice corrosion testing [7]. The specimens were immersed in the same test solutions as were used for obtaining the electrochemical data. They were dismantled and examined at the end of the tests.

The galvanic corrosion experiments were carried out in two sets, with a different artificial groundwater being used for each set of experiments, at temperatures that were representative of the long-term temperature expected in a sealed repository (i.e. 30 ºC and 50 ºC). The matrix of experiments is shown in Table 1. After the first set of experiments (i.e. Tests 1 to 4) some modifications were made to improve the design of the electrochemical cells and the datalogging systems for the second set of experiments (i.e. Tests 5 to 8).

2.2 Electrochemical cells

The experiments were carried out in standard glass electrochemical cells with the following features:

- Calomel or silver-silver chloride reference electrodes;
- Three pairs of cast iron and copper electrodes;
- An inner polyethylene container to avoid the presence of silicates which are generated by alkaline attack of glass;
- A gas tight seal which was maintained by using greased ground glass joints; however it was found to be necessary to pass a nitrogen cover gas over the test solutions to maintain a low oxygen concentration. Consequently a gas purge line was included in the cell design.

For each test environment two separate cells were set up (denoted cell A and cell B), because for electrical reasons the zero resistance ammeter (ZRA) used for the measurements only allowed one couple to be measured in each batch of electrolyte and there was a need to measure more than one couple.

Gold redox electrodes were used to give an indication of the degree of oxygenation of the solution [8]. For each test, one cast iron-copper couple was permanently coupled from the start of the experiment and one couple was connected together after a period of a few weeks corroding in the uncoupled state. A third pair of electrodes remained uncoupled throughout the test period. Figure 2 and Figure 3

show the equipment used for the second set of experiments. For each environment the following electrodes were used.

First set of experiments (Tests 1 to 4):

Cell A	Cell B
gold redox electrode calomel or silver-silver chloride reference cast iron-copper permanent couple	gold redox electrode calomel or silver-silver chloride reference uncoupled copper uncoupled cast iron copper counter electrode cast iron-copper couple after initially corroding uncoupled

Second set of experiments (Test 5 to 6):

Cell A	Cell B
gold redox electrode calomel or silver-silver chloride reference cast iron-copper couple after initially corroding uncoupled	gold redox electrode calomel or silver-silver chloride reference uncoupled copper uncoupled cast iron copper counter electrode cast iron-copper permanent couple

2.3 Electrochemical measurements

The electrochemical potentials of the coupled electrodes and the currents passing between them were measured using an ACM Instruments Galvo Gill 12 Auto ranging ZRA. This instrument automatically collected data from the galvanic couples and stored the results in a spreadsheet for further analysis

The potentials of uncoupled electrodes was logged using a separate datalogging system consisting of a high precision, high input impedance (10^9ohm) digital voltmeter (Schlumberger 7081). A Solartron Minate 7010 multiplexer unit was used to interface between the voltmeter and the electrochemical cells. This enabled eight input voltages to be scanned at periodic intervals under the control of a computer equipped with an IEEE interface card. The datalogging control programme was written in Visual Basic. The voltmeter performed a running average to obtain a six-figure reading (i.e. the resolution of the instrument was 1 μV). Six consecutive readings were displayed for each measurement. Only the last reading in each set was permanently recorded. Some potential data were also recorded using a Grant Squirrel 1200 datalogger.

The corrosion rate of uncoupled electrodes was periodically estimated from linear polarisation resistance measurements or AC impedance measurements. The corrosion rates of the test electrodes were measured using the linear polarisation resistance technique, using standard electrochemical software (Corware) and a Solartron 1286 potentiostat. Electrochemical impedance spectroscopy (EIS) was used to gain information about the capacitance (e.g. due to the double layer or surface films) and the charge transfer resistance and solution resistance.

2.4 Materials and electrode design

2.4.1 Working electrodes

Oxygen-free copper (UNS C10100, Cu-OF1) was used for the galvanic corrosion experiments. It was obtained as 12.7 mm diameter rod. The cast iron was procured according to EN 1563 (which replaces BS 2789 grade 420/12 and is equivalent to the old Swedish standard 0717). This material was obtained as 51 mm diameter round bar. The material supplier's data for the compositions of the copper and cast iron are shown in Table 2.

The specimens were machined as round-nosed bullets (Figure 1) to avoid edge effects and to allow any gas bubbles generated at the surface of the electrodes to rise to the surface. They were machined using computer controlled equipment to ensure that each specimen had the same dimensions and hence the surface area ratio for the copper to cast iron was 1:1. The exposed surface area of each specimen was approximately 10.1 cm^2. For the second set of tests the cast iron specimens used in the first set of experiments were used but it was necessary to skim the surface to remove any previous corrosion damage, resulting in a smaller diameter (~9 mm compared to the original diameter, 12 mm). For this reason the relative area Cu:Fe surface area ratio for the second set of experiments was ~1.4:1, rather than 1:1.

Electrical connection to the specimens was made by attaching 4 mm diameter threaded stainless steel rod, which was protected from exposure to the test solution using 'shrink fit' polythene sheathing. The region of the connection to the specimen was masked with a commercial masking agent ('Lacomit') for the first set of experiments, or epoxy resin (Rapid Araldite) for the second set of experiments. The sheathed threaded rods were then mounted in glass electrode connections ('Quickfit' reduction adapters) by embedding them in either Perspex cement (first set of experiments) or epoxy resin (Araldite MY753 and HY951 hardener) for the second set of experiments. The complete specimen assemblies were then mounted in a multi-neck cell head using greased ground glass conical glass joints (see Figure 3).

Prior to testing, the specimens were abraded with 600 grit abrasive paper, then degreased in acetone. The cast iron specimens were acid pickled before use to remove any surface oxide.

2.4.2 Reference electrodes

In the first set of experiments custom-made calomel electrodes (i.e. Pt/Hg/$HgCl_2$/groundwater) were prepared using plastic components to avoid dissolution of glass into the test solution. The custom-built electrodes were calibrated against standard commercial calomel electrodes. To improve reliability in the second set of experiments, the calomel electrodes were replaced by proprietary silver-silver chloride electrodes (2 mm diameter, 4 mm long sintered silver-silver chloride cylindrical pellet reference electrodes, Harvard Apparatus IVM E201) immersed directly in the test solution. Electrical connection was made to the reference electrodes by spot welding copper or Nichrome wire to the reference electrode input wire, which was then sealed and mounted in the same way as the working electrodes (see Section 2.4.1).

2.4.3 Gold redox electrodes and copper counter electrodes

The redox electrodes consisted of gold wires. Before insertion into the corrosion cell the gold was cleaned by flaming and then electrochemically treating by potential cycling in a solution of HNO_3:H_2O_2:H_2O (1:1:1 by volume) against a platinum counter electrode. The gold was cycled between +1.2V to –1.8V at a sweep rate of 10mV/s. It was then held at –1.8V for 5 minutes, washed in distilled water and transferred to the cell.

Copper gauze was used for the counter electrodes for the corrosion rate measurements. The gold wires and copper counter electrodes were mounted in the electrochemical cells in the same way as the reference electrodes.

2.4.4 Crevice specimens

The multi-crevice assembly specimens [7] consisted of a castellated cast iron nut bolted on to a flat copper specimen; the specimen design is shown in Figure 4. This specimen produced twenty small crevices between the copper and the cast iron. They were placed at the base of the test cells and were not in contact with the test electrodes.

2.5 Test solutions and test temperatures

Tests were carried out in two artificial groundwaters, namely 'bentonite-equilibrated' groundwater and Allard groundwater, and in bentonite slurry. The tests were carried out in stagnant solutions. The composition of the artificial groundwaters is shown in Table 3.

The experiments in bentonite slurry used MX-80 bentonite clay, a sodium montmorillonite, which was wetted using bentonite-equilibrated groundwater to give a composition of 30 wt% bentonite in water. This ratio of bentonite to water in the slurry was chosen because its consistency was such that it would flow easily around the test electrodes, without being excessively fluid. Freshly prepared bentonite slurry had a pH of 8.1.

The tests in the artificial groundwaters were performed at two temperatures, namely 30ºC and 50ºC. The bentonite slurry tests were carried out at 50ºC only. In the first set of experiments the test cells were mounted in an oil bath at the required test temperature. However, this approach was not ideal for producing a uniform temperature distribution, resulting in condensation at the top of the test cells and so in the second set of experiments the test cells were mounted inside ovens (one at 50ºC and one at 30ºC), as shown in Figure 2.

2.6 Oxygen concentration

The majority of the tests were performed in deaerated conditions, to simulate the expected long-term conditions in a repository. In initial experiments the cells were prepared and sealed in a nitrogen-purged glove box then transferred to the laboratory atmosphere. However preliminary experiments showed that over a period of several days a slow leakage of oxygen occurred into these cells, leading to aerobic corrosion of the cast iron as shown by the development of a brown corrosion product and therefore it was necessary to purge the cells with nitrogen to ensure low oxygen conditions. The purge gas was passed through a manifold over the top of the test solution rather than being bubbled through it. The oxygen concentration in the inlet gas was measured as 1-2 ppm. In the first set of experiments plastic tubing was used for the gas connections, but to ensure that the oxygen concentration was as low as possible for the second set of experiments the tubing was replaced by stainless steel tubing and compression fittings, with short lengths of plastic tubing used to make the final connections to glassware (see Figure 3).

The oxygen concentration in the outlet gas was measured using an oxygen meter and found to be <20 ppm. Occasionally spikes in the oxygen concentration occurred when a gas cylinder had to be changed. For a cover gas composition of nitrogen containing 2-20 ppm oxygen the oxygen concentration in solution can be calculated from Henry's law to have been in the range 0.085 to 0.85 ppb. Although this is higher than is present in the repository groundwater it is sufficiently low to demonstrate the effect of deaeration on the galvanic corrosion of copper-cast iron couples. In order to carry out tests at even lower oxygen concentrations it would be necessary to use completely sealed glass cells. The presence of corroding cast iron in the cells would have tended to reduce the oxygen concentration in the test solution.

In some experiments, the solution was initially aerated and ran for a period of a few weeks, before being deaerated. This procedure aimed to simulate the occurrence of residual oxygen in the repository and to determine the difference in galvanic corrosion behaviour between aerated and deaerated conditions and the effect of a pre-existing aerobically formed corrosion product on the surface of the cast iron.

2.7 Effect of pre-grown oxide

To investigate the effect of pre-existing corrosion product on the galvanic corrosion behaviour, the three sets of electrodes in the test cells were exposed to the following test regimes:

- couple 1 – coupled before immersion in test solution;

- couple 2 – remained uncoupled for several weeks before coupling together, to demonstrate whether the effect of a pre-grown oxide film had any effect on the galvanic corrosion currents;

- couple 3 – remained uncoupled for the whole experiment, for comparison with couples 1 and 2.

2.8 Post-test examination

After the galvanic corrosion experiments the electrodes were removed from the test cells, examined visually and photographed. The crevice corrosion specimens were dismantled and the mating surfaces were inspected and photographed.

3 Results

Unless stated otherwise the corrosion potential data are quoted with reference to the normal hydrogen electrode (NHE). The corrosion potentials were derived by taking into account the potentials of the reference electrodes measured against a standard commercial reference electrode. Current data are reported in units of μA. The area for each electrode in the first set of tests (Tests 1-4) was ~11.3 cm^2. The areas of the iron electrodes in the second set of experiments (Tests 5-8) were slightly smaller (~8.0 cm^2) because the specimens from the first set of experiments were reused and the surfaces of the cast iron specimens were skimmed to remove regions of corrosion which had developed. For the first set of experiments a current of 1 μA therefore corresponds to a current density of 0.088 $\mu A/cm^2$, which for iron corresponds to a corrosion rate of 1.02 μm/year, assuming the corrosion reaction is $Fe \rightarrow Fe^{2+} + 2e^-$. For ease of interpretation in considering the data it can be assumed that an anodic current to the iron electrode of 1 μA is approximately equivalent to a corrosion rate of 1 μm/year. For the second set of experiments 1 μA is approximately equivalent to a corrosion rate of 1.4 μm/year

3.1 Measurements in bentonite-equilibrated groundwater

The first set of experiments (Test 1 to 4) was carried out in artificial bentonite-equilibrated groundwater. The results from these experiments are shown in Figure 5 to Figure 22. The main features of the results from each of these tests are summarised below.

In Test 1 (30ºC, deaerated), there were some preliminary difficulties in obtaining a gas tight cell for the measurements and the datalogging system was still under development so there were some periods when data were not logged continuously. Nevertheless the data do show some interesting features. Air ingress caused an increase in the potential of the gold electrode and the cast iron-copper couple in Cell A (Figure 5), but the potential became more negative again either when the cell was resealed in the glovebox or a nitrogen purge over the test solution was applied. The potential of the uncoupled iron was in the range -400 to –500 mV vs NHE (Figure 6). Figure 7 shows the high dependency of the galvanic corrosion current on the presence of oxygen. After the cell was resealed inside a nitrogen-purged glovebox the galvanic corrosion current for the iron-copper couple fell from ~+100 μA to slightly negative of 0 μA, corresponding to a temporary polarity switch, as shown in the expanded scale in Figure 8. After the nitrogen purge was started the current fell rapidly and again a polarity switch was observed (i.e. the copper temporarily became the anode in the cell). Photographs of the specimens at the end of the Test 1 are shown in Figure 9.

The potentials of the electrodes in Test 2 (deaerated bentonite-equilibrated groundwater at 50ºC) are shown in Figure 10 and Figure 11. The galvanic current fell to approximately 0.1 μA on deaeration with a nitrogen purge (Figure 12 and Figure 13), while the potential of the galvanic couple fell to ~-400 mV vs NHE. Photographs of the specimens at the end of Test 2 are shown in Figure 14. It was observed that the iron specimen had taken on a copper colouration during the experiment.

The potentials of the electrodes in Test 3 (bentonite-equilibrated groundwater at 50ºC, initially aerated then deaerated) are shown in Figure 15. The galvanic current fell to less than 0.1 μA on deaeration by the nitrogen purge (Figure 16), while the potential of the galvanic couple fell to ~-600 mV vs NHE. For the couple that was connected after the copper and iron electrodes had been corroding separately, the

current during deaeration was of the order of 1.5 μA (Figure 17). The conditions of the specimens at the end of Test 3 are shown in Figure 18. A gelatinous black deposit was observed on the cast iron in the crevice specimen and on one of the coupled cast iron electrodes.

The potentials of the electrodes in Test 4 (deaerated bentonite slurry at 50ºC) are shown in Figure 19 and Figure 20. The galvanic current between the coupled cast iron and copper was of the order of 0.5 to 1 μA (Figure 21), while the potential of the galvanic couple fell to ~-450 to -500 mV vs NHE. Photographs of the specimens after removal from Test 4 are shown in Figure 22. The copper was seen to be shiny on removal from the bentonite, whereas the cast iron was covered with a black or red-brown corrosion product, indicating that there had been some residual oxygen in the test environment.

After the second set of experiments had been carried out, a repeat experiment was carried out with the bentonite-equilibrated groundwater using the modified equipment used for the second set of experiments; this was denoted Test 9. It involved setting up cells under aerated conditions at 30 °C, which was then deaerated after 647 hours. The temperature was subsequently increased to 50 °C. The results from this experiment are shown in Figure 23 and Figure 24. The results demonstrate the large reduction in galvanic current caused by deaeration and the increase in galvanic current resulting from an increase in temperature.

3.2 Measurements in Allard groundwater

The results of the measurements for Tests 5 to 8 in Allard groundwater are shown in Figure 25 to Figure 44. Some improvements to the experimental set up were made after the first set of experiments using the 'bentonite-equilibrated' water, to ensure that as much oxygen as possible was eliminated from the test cells. The data logging system was also improved. Over a period of several weeks the water level in the test cells gradually dropped due to evaporation and it was necessary to top up the test cells using deaerated deionised water. The key features of the results from each experiment are summarised below.

In Test 5 (deaerated Allard water, 30ºC) the potential of the iron in both cells A and B fell in deaerated solution and stabilised at ~-660 mV (Figure 25). It appears that deaeration occurred more rapidly in Cell A, as the potentials of the gold, copper and iron potentials fell more rapidly than in Cell B. The peaks in the potentials and currents correspond to ingress of oxygen when the nitrogen purge gas cylinders had to be changed. These peaks show that after ingress of oxygen, the oxygen was rapidly consumed by reaction with the test electrodes and the potentials fell to their previous values in deaerated conditions. The potentials of the permanently coupled electrodes for Test 5 (Figure 26) were also ~-660 mV, showing that the potential of the couple was dominated by the cast iron rather than the copper. Some electrical noise was experienced in the potential measurements (e.g. gold electrodes and iron-copper couple in cell B). The current passing between the permanently coupled electrodes (Cell B, Figure 26 and Figure 27) fell to very low values (<0.1 μA) and on occasions the polarity of the current switched, indicating that the copper had become the anode (see Figure 27). It appears that there was a bad contact in the electrical circuit between 2,000 and 2,500 hours exposure (see Figure 26). The current passing between the electrodes that were initially corroded uncoupled, then coupled are shown in Figure 28. This figure also shows a transient due to temporary ingress of oxygen. A further experiment was carried out on this couple, and the permanently coupled couple, in which the temperature was increased to 50 ºC to determine whether there was any direct effect on the galvanic current. The results of this experiment are shown in Figure 29 and Figure 30. Photographs of the specimens after removal from Test 5 are shown in Figure 31. The copper specimens were generally shiny and the cast iron specimens were covered with a thin black corrosion product.

The potentials of the electrodes in deaerated Allard water at 50ºC (Test 6) are shown in Figure 32. The potential of the iron electrodes was typically ~-680 mV to – 700 mV with some positive excursions during oxygen ingress. These values are slightly more negative than at 30ºC. The potentials of the gold and copper electrodes in cells A and B were similar, and similar to cell A at 30ºC, but more positive than in cell B at 30ºC. The galvanic currents at 50ºC (Figure 33 and Figure 34) were generally higher at 50ºC than at 30ºC (typically 1-2 μA between oxygen ingress events at 50ºC,

compared to <0.1 μA at 30ºC). The currents passing between the couples that were originally corroding uncoupled are shown in Figure 35. Photographs of the specimens after removal from Test 6 are shown in Figure 36.

The potentials of the electrodes in aerated Allard water at 50ºC, which was subsequently deaerated, (Test 7) are shown in Figure 37 and the corresponding current measurements are shown in Figure 38 (note: the galvanic current data became very noisy, probably due to a bad contact, after 1650 hours exposure and these data are not shown). In aerated conditions the potentials of the gold and copper electrodes exhibited a general trend to more negative values after deaeration started, with frequent transients in the potential superimposed on the general downward trend. The current data show that in aerated solutions the galvanic currents were much higher than in deaerated conditions (of the order of 100 μA in aerated conditions cf. 1-2 μA in deaerated conditions). The current passing between specimens that were not initially coupled together are shown in Figure 39. The minimum current measured before a fresh oxygen transient was ~0.2 μA. The condition of the specimens after removal from Test 7 is shown in Figure 40. The copper was generally uncorroded, but stained with black corrosion product from corrosion of the cast iron.

The potentials of the electrodes in bentonite slurry at 50ºC which was initially aerated and subsequently deaerated (Test 8), are shown in Figure 41 and the corresponding current measurements are shown in Figure 42. The currents passing to specimens that were initially uncoupled are shown in Figure 43. The condition of the specimens after removal from Test 8 is shown in Figure 44. There was a layer of reddish-brown corrosion product which is assumed to have formed when conditions were aerated, but a layer of black corrosion product was visible underneath. A green corrosion product was visible on the copper, which is assumed to have been formed in the presence of oxygen prior to deaeration.

4 Discussion

4.1 Effect of oxygen concentration

In the presence of oxygen, copper was the cathode in the cast iron-copper couples. This is in agreement with published results for the galvanic corrosion of copper-iron couples in aerated seawater. For example, reference [9] gives the galvanic series in flowing seawater, in which the potential of mild steel or cast iron is in the range -360 to –460 mV vs NHE and that of copper is -60 to –110 mV vs NHE. This range of iron potentials is consistent with the values measured in the present work in aerated conditions (e.g. Figure 15 and Figure 24), although the potential of the copper measured in aerated artificial groundwaters tended to be more positive than the values given in the literature for seawater.

The copper and iron potentials measured in the present work in deaerated conditions were considerably more negative than in aerated conditions (e.g. see Figure 25), but the iron mainly remained more negative than the copper, indicating that iron would be the anode in any galvanic couple in deaerated conditions. Occasionally the potential of copper fell below that of iron (e.g. Figure 10) and this would explain why sometimes there was a polarity reversal and the copper became the anode in the couple (e.g. Figure 12). The potential of the iron was below the hydrogen evolution potential at the pH of the groundwaters (-383 mV vs NHE at pH 9 and –443 mV vs NHE at pH 10, 0.00001 atm H_2) and so hydrogen evolution by anaerobic corrosion of the iron was thermodynamically possible. The potential of the copper in deaerated conditions was within the thermodynamic domain of stability for copper, according to the Pourbaix diagram for copper [10]. In aerated conditions the copper was in a potential regime where copper oxide could form (i.e. the copper was corroding). The observation of copper plating on the surface of the iron specimen in Test 2 (Figure 14) is indicative of dissolved copper in the test solution, produced as a result of transient aerobic corrosion, which then plated out on the surface of the iron.

Mansfeld and Kenkel [11] investigated the galvanic corrosion of a range of dissimilar metal couples, including 4130 steel and copper, over a period of 24 hours in naturally aerated 3.5% NaCl. The

results for a copper-4130 steel couple are summarised in Table 4. They show that the corrosion rate of steel was increased by a factor of ×13 when coupled to a copper electrode. This was attributed to the copper being an efficient cathode for the reduction of oxygen. They showed that the increase in corrosion current due to galvanic coupling can be described by:

$$i_g^A = i_a^A - i_{corr}^A \quad (1)$$

where i_g^A is the increase in the dissolution rate due to galvanic coupling, i_a^A is the dissolution current density of the coupled anode material and i_{corr}^A is its corrosion current density when uncoupled (i.e. freely corroding). This behaviour can also be presented in terms of dissolution rates:

$$R_G = R_A - R_0 \quad (2)$$

where R_G is the increase in corrosion rate due to coupling, R_A is the total anodic dissolution rate (equivalent to the corrosion rate due to weight loss, R_{WL}), and R_0 is the uncoupled corrosion rate.

Similarly, Astley and Scholes [12] found that iron was the anode in copper-mild steel couples in aerated seawater, with a corrosion rate for a 1:1 area ratio of 270 µm/year, based on weight loss data. This represented an acceleration factor of ~×3, compared to the corrosion rate of uncoupled mild steel. The enhancement in galvanic corrosion depends on the relative areas of copper and steel: the galvanic current is proportional to the area of the cathodic metal [12,13]. Other workers have also found an acceleration of the corrosion rate of carbon steel when galvanically coupled to copper alloys at high temperatures in concentrated aerated brines, in relation to the German nuclear waste disposal programme [14]. To the authors' knowledge, no electrochemical measurements on the copper-iron system in deaerated groundwater have been reported in the open literature.

In the experiments reported here the galvanic corrosion current in aerated conditions was equivalent to an i_g^A value of ~100 µm/year (e.g. Figure 38), which is similar to the values reported for copper-mild steel couples in seawater. However, when the solutions were deaerated, the galvanic corrosion current was greatly reduced. For example, at 30ºC galvanic corrosion rates as low as 0.02 µm/year for iron were observed after deaeration (Figure 28). There was a correlation between the amount of oxygen present and the galvanic corrosion current, as shown by the fact that oxygen induced potential transients led to transient increases in the galvanic corrosion current (e.g. Figure 28). In deaerated conditions the cathodic reaction is the reduction of water rather than oxygen and the corrosion rate is initially determined by the kinetics, or the activation overpotential, of the hydrogen evolution reaction on the cathode. Oxygen is a far more powerful oxidant for iron than water because of the greater separation in the thermodynamic equilibrium potentials for iron dissolution and oxygen reduction and therefore the corrosion rates are higher in aerated conditions.

The galvanic corrosion rates measured in deaerated conditions were similar to the long-term anaerobic corrosion rates measured using barometric gas cells to collect hydrogen [15-17], which were of the order of 0.1 – 1 µm/year. Furthermore, gas generation experiments using pieces of steel and copper wire spot-welded together failed to produce any increase in hydrogen generation rate [3]. These results indicate that in the absence of oxygen the long-term corrosion rate is determined by the formation of a corrosion product film on the surface of the iron and not by the kinetics of the cathodic reaction on the surface of the copper and/or the iron. This result is consistent with previous measurements [3] and predictions based on the theory of galvanic coupling [2].

The potential of the iron electrode was much less affected by fluctuations in oxygen concentration than copper or gold. This is similar to the behaviour seen previously in sealed glass cells [8], where the potentials were similar to those observed in the present work for iron, copper and gold in fully deaerated conditions (e.g. Figure 25). It appears that because the copper and gold do not have a surface oxide film they are more easily perturbed by small local variations in the chemical conditions than the iron electrode, which does have a surface oxide film.

4.2 Effect of exposure time

With increased exposure time, there was a general reduction in the corrosion rate of iron coupled to copper in deaerated conditions and this was probably due to the slow accumulation of a corrosion product layer, as shown by the appearance of a black film on the surface of the iron electrodes. This corrosion product probably consisted of magnetite (Fe_3O_4), as this was the composition of the black oxide observed previously in experiments to measure the expansion of a stack of galvanically coupled copper and steel discs under similar anoxic conditions [18,19]. This view is supported by the fact that the potential of the electrodes under deaerated conditions was in the potential region in the iron Pourbaix diagram that corresponds to magnetite formation [20,21]. The potentials also correspond to the potential domain for ferrous hydroxide and it is possible that this was the initial reaction product, which subsequently transformed to magnetite via the Schikorr reaction. It is normally accepted that this transformation only occurs at temperatures above 85 °C, although magnetite has been observed in other low temperature anaerobic corrosion experiments with iron [22].

4.3 Effect of temperature

The effect of temperature on the corrosion rate can be observed by comparing the galvanic current data obtained at 30 ºC and 50 ºC (e.g. Figure 26, Figure 30, Figure 34 and Figure 35) and by examining the results from the experiments where the temperature was increased during the course of the experiments (Figure 23, Figure 29 and Figure 30). These data show that increasing the temperature causes an increase in the galvanic corrosion current in deaerated environments by up to a factor of approximately ×10. Increasing the temperature has also been observed to cause an increase in the rate of production of hydrogen caused by anaerobic corrosion of iron [15,17]. The increase in the galvanic current caused by increasing the temperature can be attributed to increasing the exchange current density for the water reduction reaction on the copper cathode and to an increase in the rate of diffusion processes in the oxide film. It is probable that there was a similar increase in the water reduction current on the surface of the iron, but this would not have been detected by the ZRA.

4.4 Effect of pre-existing corrosion product

Figure 28 shows the currents passing after a specimen that had been corroding anaerobically in Allard water at 30 ºC was coupled to copper. The corrosion current remained at a low value, which was at least as low as for a specimen that was permanently coupled from the start of the experiment (Figure 27) in the same test solution (Figure 30). Similar behaviour can be seen for anaerobically pre-corroded specimens (Figure 34 and Figure 35) and aerobically pre-corroded specimens (Figure 39), for Allard water at 50 ºC. The delayed coupling of electrodes in bentonite slurry (Figure 43) yielded higher corrosion rates than in comparable aqueous conditions, but they were similar to permanently coupled specimens in bentonite slurry (Figure 42).

4.5 Effect of bentonite slurry

The data obtained in bentonite slurry tended to be rather erratic (e.g. Figure 19-Figure 21 and Figure 41-Figure 43) compared to the data from aqueous solutions. This may reflect the difficulties in removing dissolved oxygen from a slurry of bentonite and/or the effect of bentonite on the stability of immersed reference electrodes. The galvanic currents measured in Tests 4 and 8 using bentonite slurry were generally higher than in comparable aqueous experiments. This could be due to higher residual oxygen concentrations in the bentonite slurry, but it is also consistent with the higher anaerobic corrosion rates observed in hydrogen generation experiments on steel embedded in compacted bentonite [23]. The reasons for the enhanced corrosion rate of carbon steel in bentonite are the subject of ongoing investigations.

4.6 Effect of groundwater composition

Within the experimental scatter it was not possible to distinguish between the galvanic corrosion rates in the Allard groundwater and the bentonite-equilibrated groundwater. Other work has shown that the anaerobic corrosion rate of carbon steel in anoxic alkaline solutions is insensitive to chloride concentration [24], but the corrosion rate would be expected to be lower in the bentonite-equilibrated groundwater, which has a slightly higher pH [15,17] (see Table 3).

4.7 Effect of specimen area

It has been shown by other workers that in aerated conditions there is a distinct effect of the relative areas of the coupled copper and iron electrodes on the galvanic corrosion rate. For example, Whitman and Russell [13] showed that the galvanic current is directly proportional to the area of the cathodic metal, but independent of the area of the anodic metal. Similarly, on the basis of weight loss measurements, Astley [12] reported galvanic corrosion rates for mild steel in mild steel-copper couples of 0.11, 0.27 and 6.7 mm $year^{-1}$ for mild steel-copper area ratios of 10:1, 1:1 and 1:10 respectively. However, in deaerated conditions, where the corrosion rate appears to be determined by the properties of the corrosion product film it is likely that there will be little effect of relative areas of coupled iron and copper, although this factor was not examined experimentally in the present work.

4.8 Effect of crevices

When the castellated nut crevice samples were dismantled there was no evidence of crevice attack of either the cast iron or the copper. Where oxygen had been present in the test cell, copious quantities of corrosion product were observed on the cast iron specimens. In fully deaerated conditions a thin black film was present on cast iron. It would be expected that conventional crevice corrosion, as observed in aerated conditions, would not be able to take place under anaerobic conditions, due to the lack of an external cathodic reaction. In anoxic conditions water reduction could take place on surfaces both within and external to the crevice, whereas in oxygenated conditions the thermodynamic driving force for crevice corrosion is greater and the cathodic reaction occurs on the outside surface. The results from the castellated nut specimens can be compared with those from the experiments to study possible corrosion-induced expansion [18,19], where a stack of copper and cast iron or steel washers was placed under load and corroded anaerobically. In the latter experiments, although copious quantities of black corrosion product were observed on the cast iron, no enhanced corrosion of the copper was detected.

4.9 Application of results to assessment of SKB canister performance

In terms of application of the results presented in this report to the evolution of the environment within the annulus of the canister the following scenario is envisaged. If water penetrates the annulus through a hole in the outer copper container a galvanic couple will be set up between the copper and the cast iron insert. The current passing between the copper and the cast iron will be concentrated at the contact points. If any residual air is present in the annulus the corrosion rate of the cast iron will be enhanced (i.e. the iron will be the anode and copper the cathode). The measured galvanic corrosion currents passing to the iron in fully aerated artificial groundwater were equivalent to corrosion rates in the region of 100 μm/year. In the absence of oxygen in the annulus, as a result of oxygen consumption by corrosion of the cast iron insert or by reaction with the surrounding matrix, the galvanic corrosion currents will fall markedly. The galvanic corrosion rates of iron coupled to copper at low groundwater oxygen concentrations have been measured as <0.1 μm/year at 30ºC and <1 μm/year at 50ºC. These are close to the values observed for anaerobic corrosion rates of uncoupled iron. The cast iron normally remains the anode in the galvanic couple although temporary polarity reversal has been observed at very low currents. In the event of a breach in the outer copper canister, the relative areas of the copper and cast iron affected by galvanic corrosion would be expected to be similar, so the data reported here for ~1:1 area ratios are relevant.

5 Conclusions

The main conclusions from this work are as follows:

1. For copper-cast iron couples in artificial groundwaters simulating the SKB repository environment, deaeration leads to a marked decrease in the galvanic corrosion of iron.

2. The corrosion rates in deaerated conditions were comparable to those measured for iron corroding in the absence of galvanic coupling to copper.

3. Under deaerated conditions a black film was formed on the surface of the cast iron, which was consistent with the formation of magnetite. The electrochemical potentials of the cast iron-copper couples in deaerated conditions were in the thermodynamically stable regions for magnetite and metallic copper.

4. Increasing the temperature from 30 ºC to 50 ºC led to an increase in the galvanic corrosion current in deaerated environments by a factor of up to $\times$10.

5. The presence of bentonite appears to increase the galvanic corrosion current compared to aqueous solutions.

6. Pre-grown corrosion films on cast iron did not have a significant effect on subsequent measured galvanic corrosion rates when coupled to copper.

7. No galvanically enhanced crevice corrosion was observed when copper and cast iron were coupled in deoxygenated conditions.

6 Recommendations for further work

On the basis of the experiments reported here the following recommendations for possible future work are made:

1. In order to reduce the oxygen content of the test environments to lower levels, a small number of experiments could be carried out in completely sealed custom-built glass cells, similar to those used in reference [8].

2. The effect of relative electrode areas on the galvanic current under anoxic conditions could be investigated to confirm that there is no significant effect.

3. The effect of bentonite on galvanic corrosion could be investigated further using compacted bentonite to embed the samples.

4. Other factors that might affect corrosion, and which have been raised in a review of galvanic corrosion performed for SKI [4], include the effect of sulphides, impurities in the copper and the presence of microbes on galvanic corrosion behaviour. These parameters could be investigated using the techniques applied in the present work.

5. Consideration could be given to applying mathematical modelling techniques to predicting the effect of various parameters on galvanic corrosion and comparing to the results from experimental investigations. This approach has been used by other workers to improve mechanistic understanding of the iron-copper galvanic corrosion processes [25,26].

6. The presence of a radiation field could in principle lead to the formation of oxidising species, such as peroxide, which might affect the galvanic corrosion rate by providing an additional cathodic reactant. This effect could either be investigated by subjecting test cells to a radiation

field in a radiation cell, or by adding some of the products expected to be produced by radiation to the test environment. Clearly, the latter is less realistic but simpler to achieve experimentally and it may be sufficient to show whether an effect is likely. The first step would be to calculate how much peroxide might be formed through radiolysis.

7 References

1 D.J. Blackwood, A.R. Hoch, C.C. Naish, A. Rance and S.M. Sharland, *Research on Corrosion Aspects of the Advanced Cold Process Canister*, AEA Technology Report, AEA-D&W-0684, pg. 18, 1994. Also available as SKB Technical Report 94-12.

2 D.J. Blackwood and C.C. Naish, *The Effect of Galvanic Coupling Between the Outer Copper Canister and the Carbon Steel Inner Canister on the Corrosion Resistance of the Advanced Cold Process Canister*, AEA-ESD-0053, 1994. Also available as SKB Inkapsling Projektrapport 95-04.

3 D.J. Blackwood, C.C. Naish and A.P. Rance, *Further Research on Corrosion Aspects of the Advanced Cold Process Canister*, AEA Technology Report, AEA-ESD-0052, 1994. Also available as SKB Inkapsling Projektrapport 95-05.

4 H-P. Hermansson, *Galvanic and Stress Corrosion of Copper Canisters in Repository Environment. A Short Review*, Swedish Nuclear Inspectorate SKI Report 01:38, 2001.

5 *Standard Guide for Conducting and Evaluating Galvanic Corrosion Tests in Electrolytes*, ASTM G 71-81(1998)e1.

6 *Standard Guide for Development and Use of a Galvanic Series for Predicting Galvanic Corrosion Performance*, ASTM G 82-98.

7 *Standard Guide for Crevice Corrosion Testing of Iron-Base and Nickel-Base Stainless Alloys in Seawater and Other Chloride-Containing Aqueous Environments*, ASTM G 78-01.

8 R. Peat, S. Brabon, P.A.H. Fennell, A.P. Rance and N.R. Smart, *Investigation of Eh, pH and Corrosion Potential of Steel in Anoxic Groundwater*, AEAT/R/PS-0028, issue 1, 2000 and SKB report TR-01-01, 2001.

9 F.L. LaQue, *Galvanic Corrosion*, chapter 6 in 'Marine Corrosion', John Wiley, 1975.

10 N. de Zoubov, C. Vanleugenhaghe and M. Pourbaix, *Copper*, Section 14.1 in 'Atlas of Electrochemical Equilibria in Aqueous Solutions', M. Pourbaix (ed.), N.A.C.E. / Cebelcor, 2nd edition, pg. 384, 1974.

11 F. Mansfeld and J.V. Kenkel, *Laboratory Studies of Galvanic Corrosion I. Two-Metal Couples*, Corrosion **31**(8), 1975.

12 D.J. Astley and I.R. Scholes, *Bimetallic Corrosion in Seawater*, SMCC/7/74, report by Imperial Metal Industries for UK MoD, technical report 5/74, October 1974.

13 W.G. Whitman and R.P. Russell, *The Natural Water Corrosion of Steel in Contact with Copper*, Ind. Eng. Chem. **16**, 276, 1924.

14 E. Smailos and B. Kienzler, *Galvanic Corrosion Between the nuclear Waste Disposal Container Materials Copper-Nickel Alloys and Carbon Steel in Salt Brines*, Corrosion 2004, Paper 04688, N.A.C.E., Houston, 2004.

15 N.R. Smart, D.J. Blackwood and L. Werme, *The Anaerobic Corrosion of Carbon Steel and Cast Iron in Artificial Groundwaters*, SKB Report TR-01-22, 2001.

16 N.R. Smart, D.J. Blackwood and L. Werme, *Anaerobic Corrosion of Carbon Steel and Cast Iron in Artificial Groundwaters: Part 1–Electrochemical Aspects*, Corrosion **58**(7), 547, 2002.

17 N.R. Smart, D.J. Blackwood and L. Werme, *Anaerobic Corrosion of Carbon Steel and Cast Iron in Artificial Groundwaters: Part 2-Gas Generation*, *Corrosion* **58**(8), 627, 2002.

18 N.R. Smart, A.E. Bond, J.A.A. Crossley, P.C. Lovegrove and L. Werme**,** *Mechanical Properties Of Oxides Formed By Anaerobic Corrosion Of Steel*, Materials Research Society Symposium Proceedings Volume 663, Scientific Basis for Nuclear Waste Management XXIV, K.P. Hart and G.R. Lumpkin (eds), p. 477-485, 2001.

19 N.R. Smart, A.P. Rance, P. Fennell and L. Werme, *Expansion due to Anaerobic Corrosion of Steel and Cast Iron: Experimental and Natural Analogues Studies*, in 'Prediction of Long Term Corrosion Behaviour in Nuclear Systems', D. Féron and D.D. Macdonald (eds), European Federation of Corrosion Publications Number 36, 2003.

20 M. Pourbaix and N. de Zoubov, *Iron*, Section 12.1 in 'Atlas of Electrochemical Equilibria in Aqueous Solutions', M. Pourbaix (ed.), N.A.C.E. / Cebelcor, 2nd edition, pg. 307, 1974.

21 H-P Hermansson, *The Stability of Magnetite and Its Significance as a Passivating Film in the Repository Environment*, SKI report 2004:07, 2004.

22 A.P. Rance, R. Peat and N.R. Smart, *Analysis of Electrochemistry Cells*, Serco Assurance report SA/RJCB/62036/R01, 2003. Also available as SKB report TR-04-01.

23 N.R. Smart, A.P. Rance and L.O. Werme *Anaerobic Corrosion of Steel in Bentonite*, Materials Research Society Symposium Proceedings Volume 663, Scientific Basis for Nuclear Waste Management XXVII, V.M. Oversby and L.O. Werme (eds.), p. 441-446, 2004.

24 N.R. Smart, D.J. Blackwood, G.P. Marsh, C.C. Naish, T.M. O'Brien, A.P. Rance and M.I. Thomas, *The Anaerobic Corrosion of Carbon and Stainless Steels in Simulated Cementitious Repository Environments: A Summary Review of Nirex Research*, AEAT/ERRA-0313, 2004.

25 C.R. Crowe and R.G. Kasper, *Ionic Current Densities in the Nearfield of a Corroding Iron--Copper Galvanic Couple*, Journal of the Electrochemical Society, **133**(5), 879-887, 1986.

26 D.S. Dunn and G.A. Cragnolino, *Effect of Galvanic Coupling Between Overpack Materials of High-Level Nuclear Waste Containers – Experimental and Modeling Results,* CNWRA 98-004, 1998.

Test number	Artificial groundwater	Test temperature (ºC)	Oxygenation
1	Bentonite-equilibrated	30	fully deaerated
2	Bentonite-equilibrated	50	fully deaerated
3	Bentonite-equilibrated	50	aerate then deaerate
4	bentonite slurry	50	fully deaerated
5	Allard	30	fully deaerated
6	Allard	50	fully deaerated
7	Allard	50	aerate then deaerate
8	bentonite slurry	50	aerate then deaerate

Table 1. Matrix of galvanic corrosion experiments

Material	C	Si	Mn	S	P	Mg	Fe	Cu	Pb	Hg
Cast iron – BS 2789 grade 420/12	3.69	2.72	0.112	0.013	0.032	0.071	bal			
Copper ASTM C101					2 ppm			99.99% min	4 ppm	<1

Table 2. Composition of test materials for galvanic corrosion experiments (wt%)

Ion	Bentonite-equilibrated water		Allard water	
	mM	**ppm**	**mM**	**ppm**
Na^+	560	12880	to match pH 9.0 (~206)	
Cl^-	540	19170	195	6940
HCO_3^-			1	61
CO_3^{2-}	10	600		
SO_4^{2-}			5	480
pH	10.4		9.0*	

*pH was adjusted by addition of NaOH.

Table 3. Composition of artificial groundwaters used for galvanic corrosion experiments

	Copper	4130 steel
Ecorr (mV vs SCE)	–237 ±10	–591 ±19
Average galvanic current density in couple ($\mu A\ cm^{-2}$)	-28.8	+27.4
Corrosion rate from wt loss of uncoupled metals, R_0, ($mg\ dm^{-2}\ day^{-1}$, mdd)	N/A	18.0
Corrosion rate from wt loss in couple, R_{WL}, ($mg\ dm^{-2}\ day^{-1}$, mdd)	0.5	252.8
Corrosion rate based on galvanic current and Faraday's law ($mg\ dm^{-2}\ day^{-1}$, mdd)	N/A	68.5
Acceleration of corrosion rate due to galvanic coupling, $(R_{WL} - R_0)/R_0$	N/A	13.0

Table 4. Summary of results from Mansfeld and Kenkel [11] on galvanic couples of copper and 4130 carbon steel over a period of 24 hours in naturally aerated 3.5% NaCl.

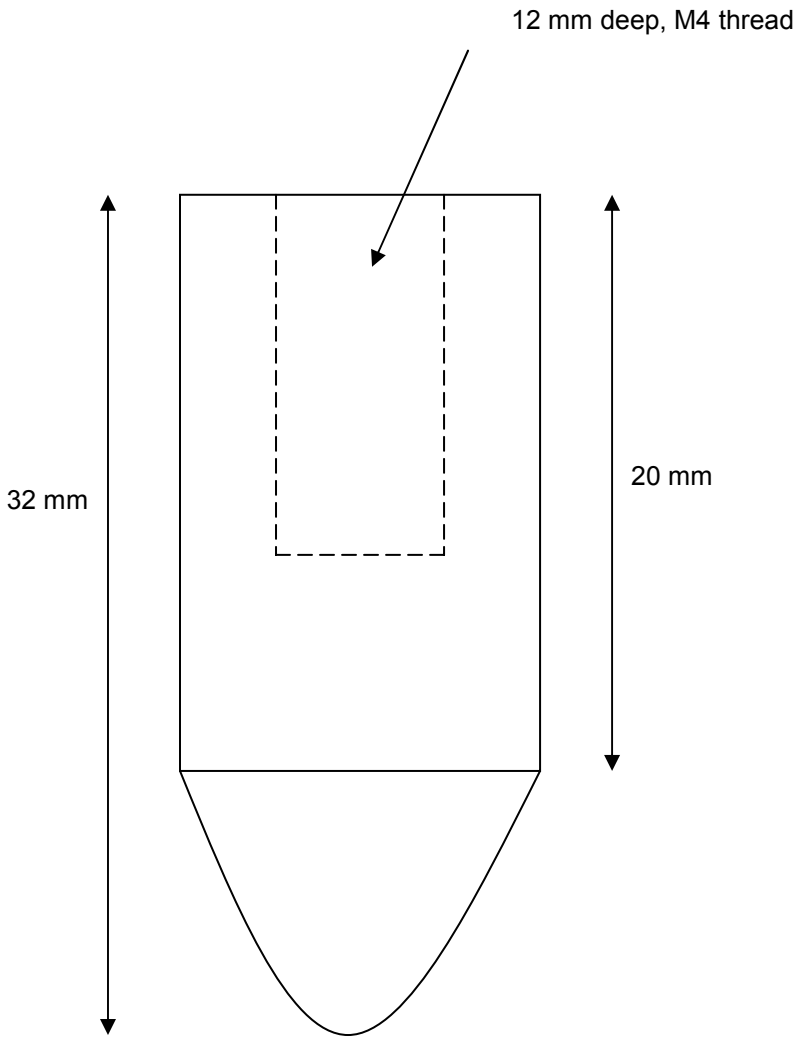

Figure 1. Design of bullet specimens for galvanic corrosion experiments.

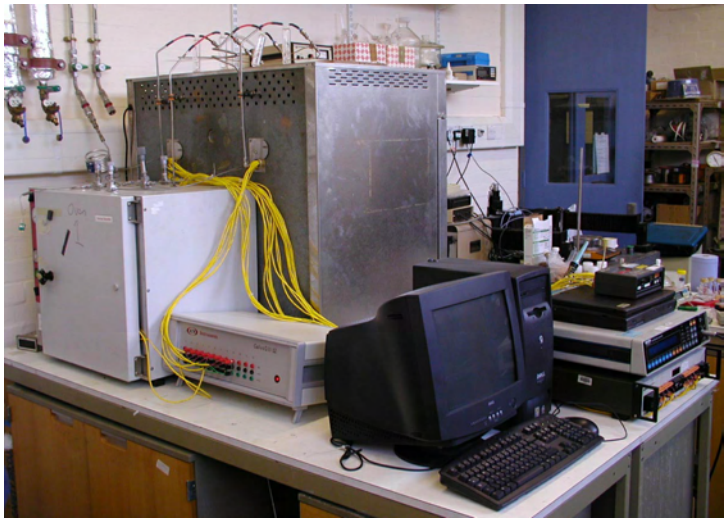

Figure 2. Equipment used for second set of galvanic corrosion experiments

Figure 3. Photographs of electrochemical cells used for second set of galvanic corrosion experiments.

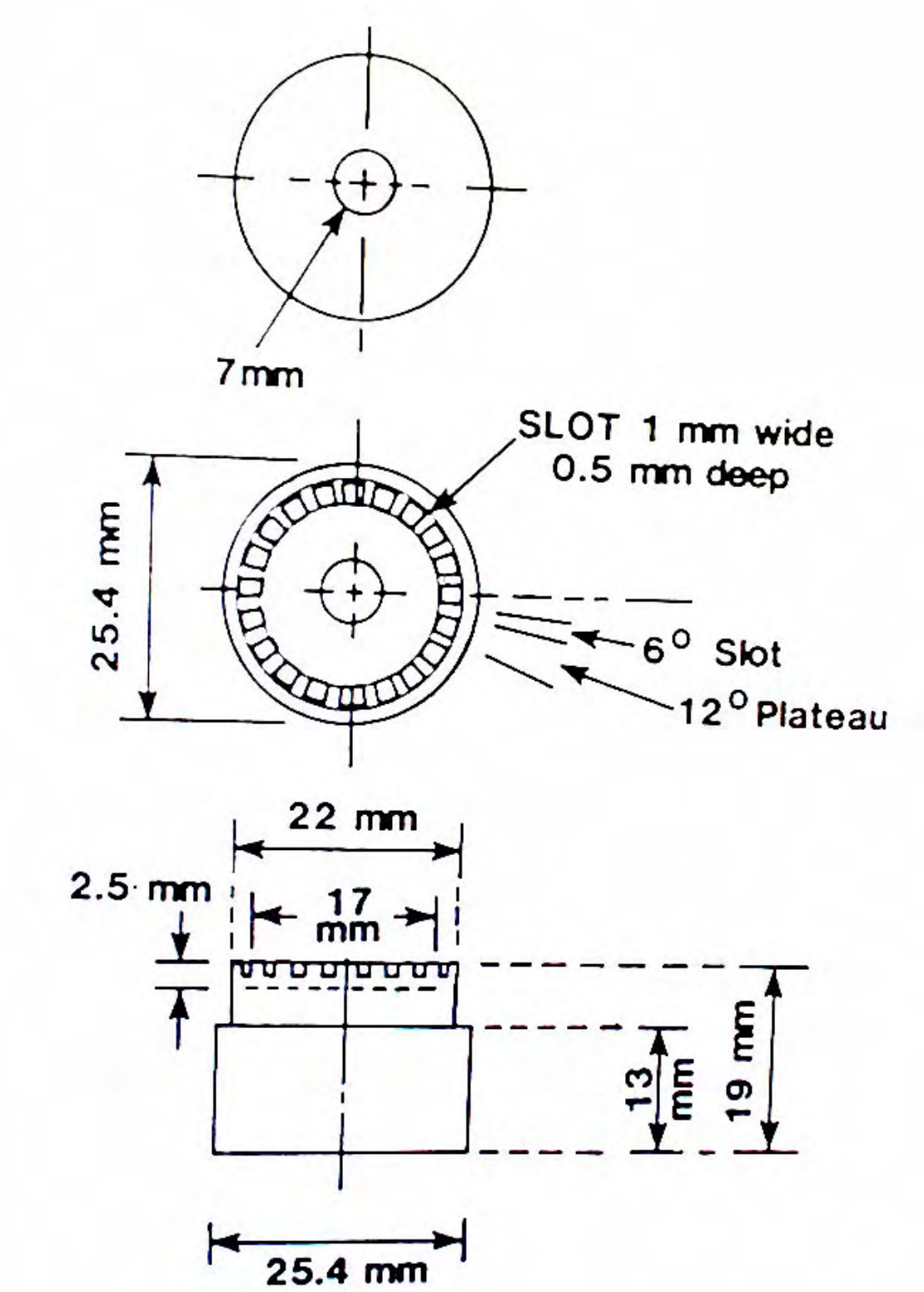

Figure 4. Details of multiple crevice assembly design (from [7])

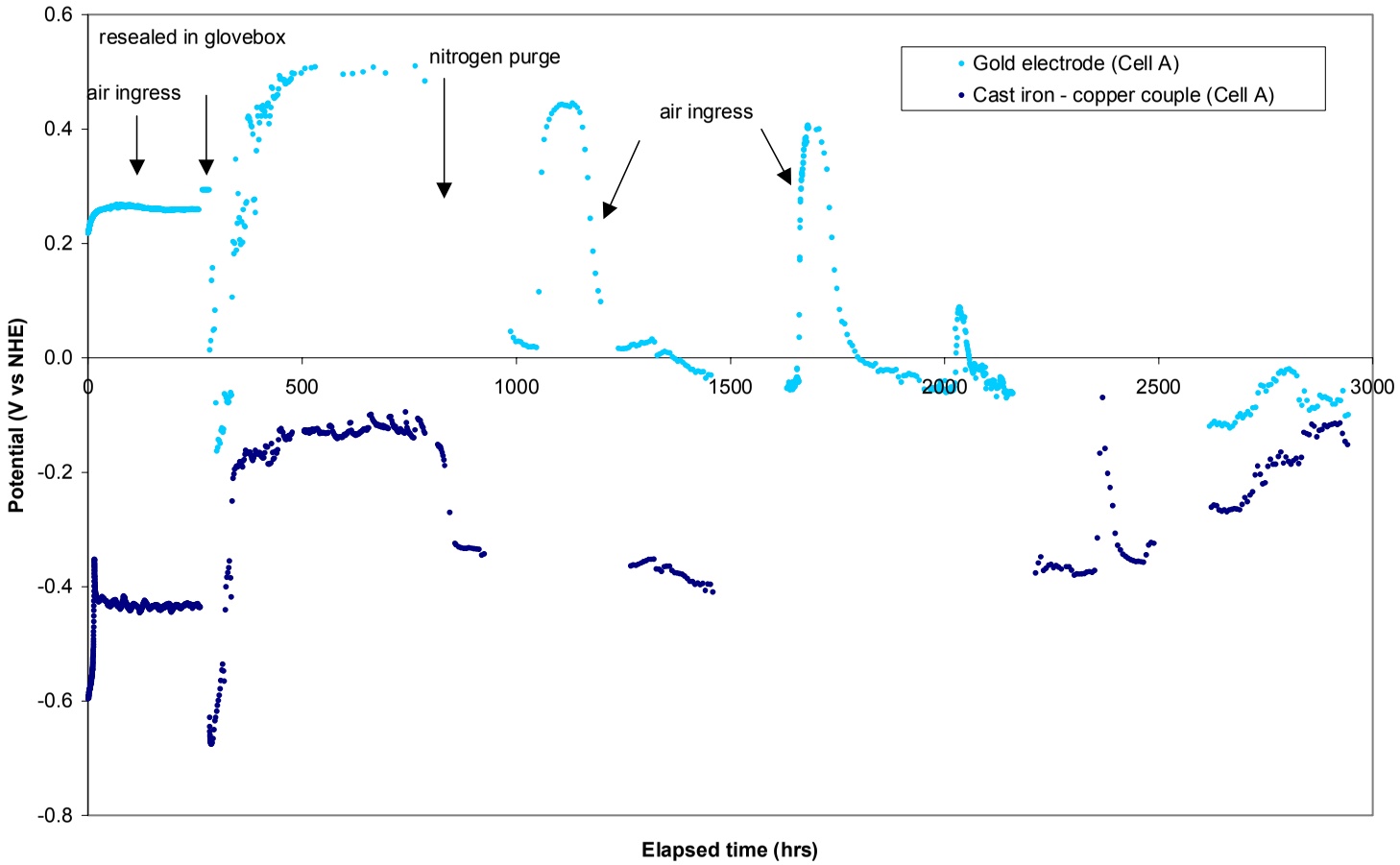

Figure 5. Potential of electrodes in deaerated bentonite-equilibrated groundwater at 30ºC (Test 1, Cell A).

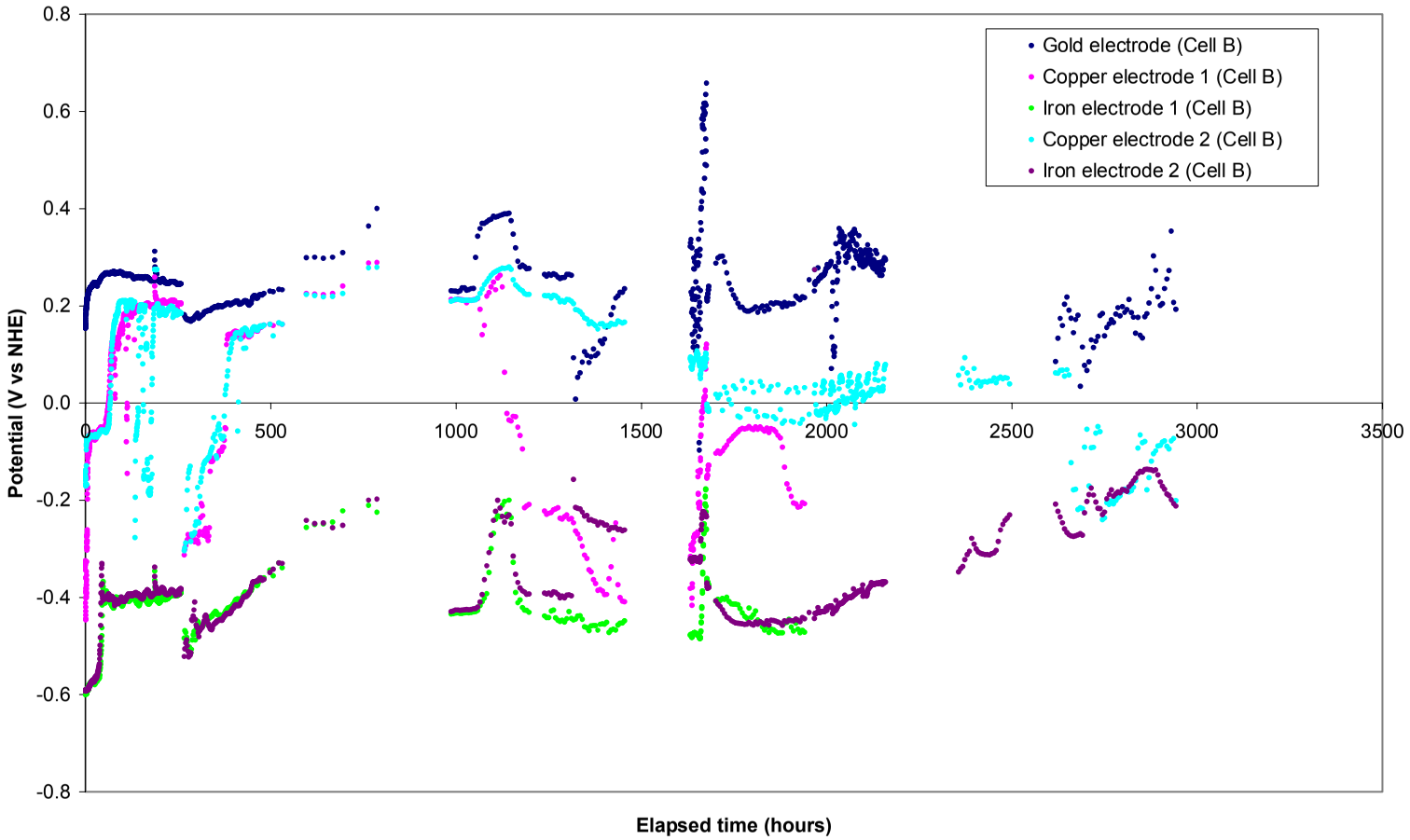

Figure 6. Potential of electrodes in deaerated bentonite-equilibrated groundwater at 30ºC (Test 1, Cell B).

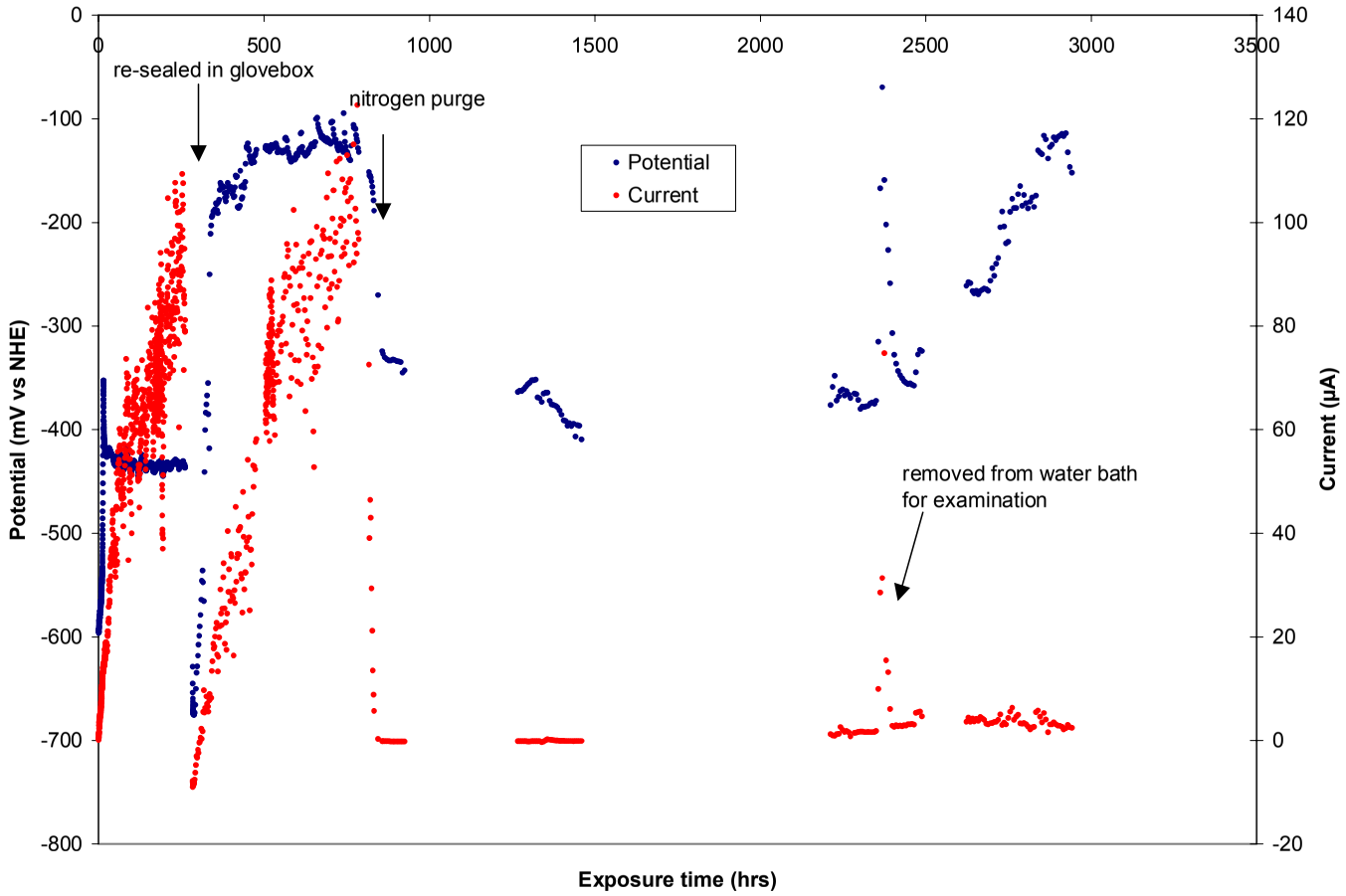

Figure 7. Currents passing between permanently coupled cast iron and copper electrodes in deaerated bentonite-equilibrated groundwater at 30º C, and potential of coupled electrodes (Test 1, Cell A).

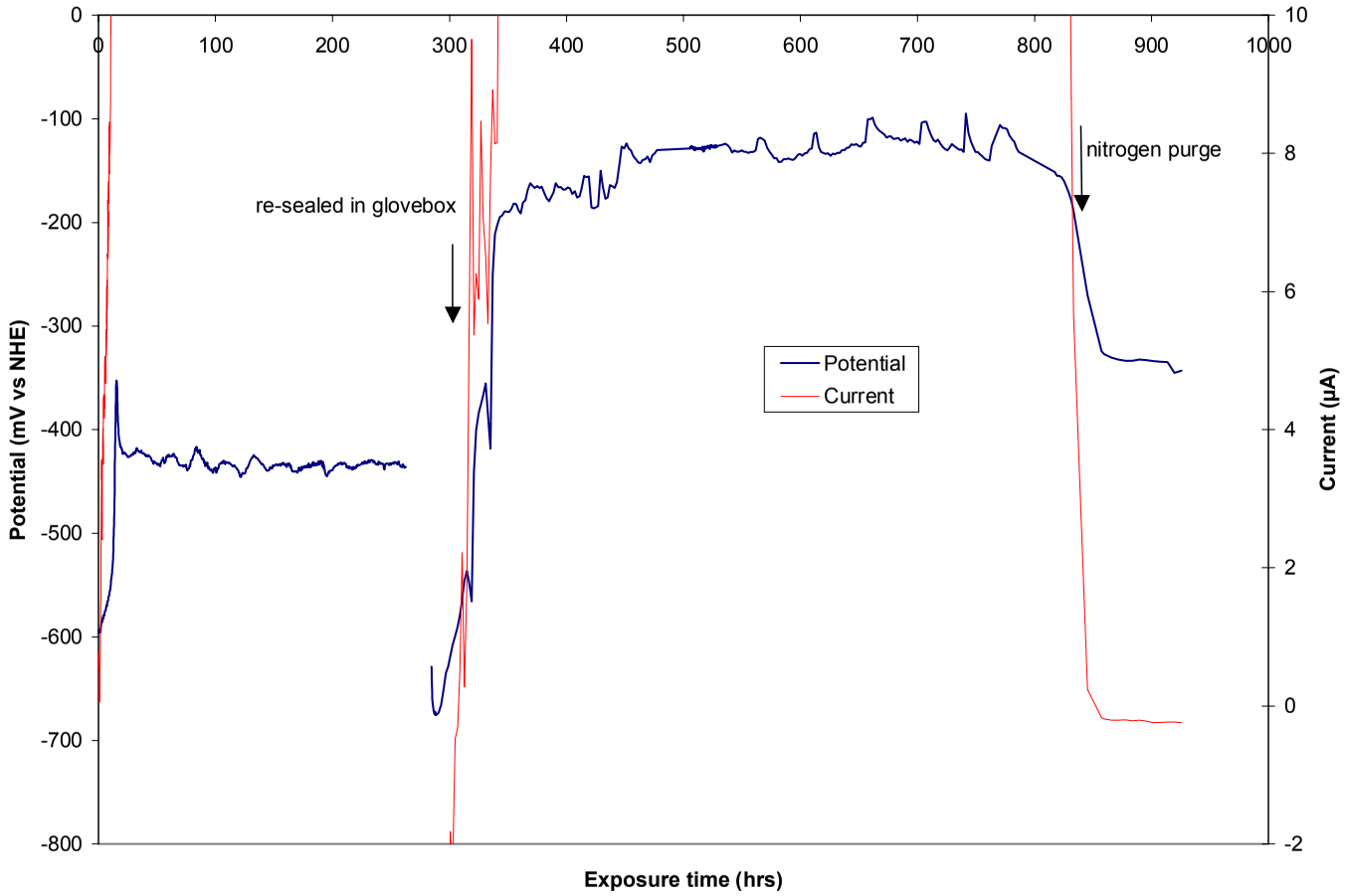

Figure 8. Currents passing between permanently coupled cast iron and copper electrodes in deaerated bentonite-equilibrated groundwater at 30º C, and potential of coupled electrodes (Test 1, Cell A), expanded scale.

Figure 9. Specimens at the end of Test 1 (deaerated bentonite-equilibrated groundwater at 30º C).

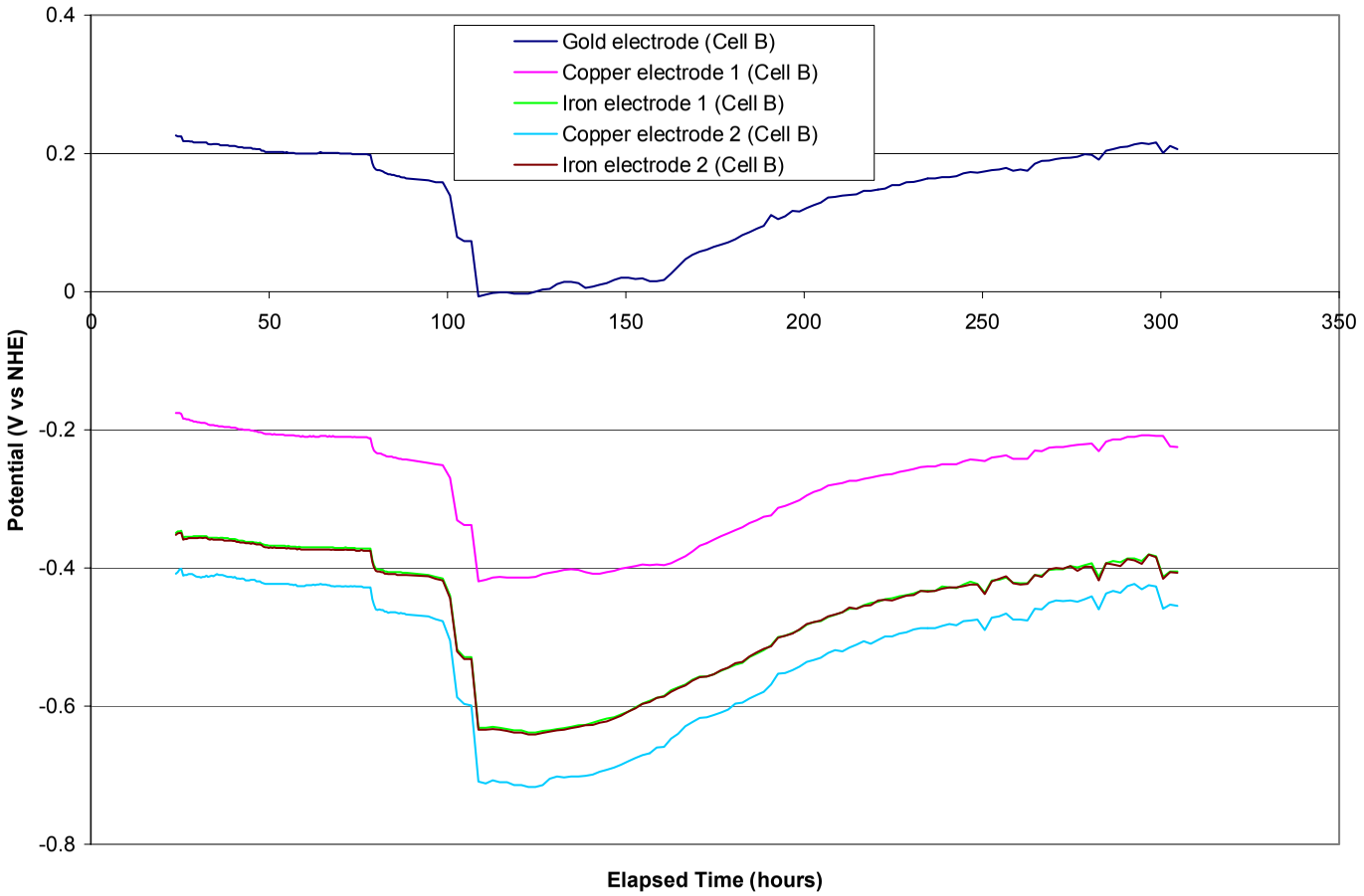

Figure 10. Potential of electrodes in deaerated bentonite-equilibrated groundwater at 50°C (Test 2, Cell B).

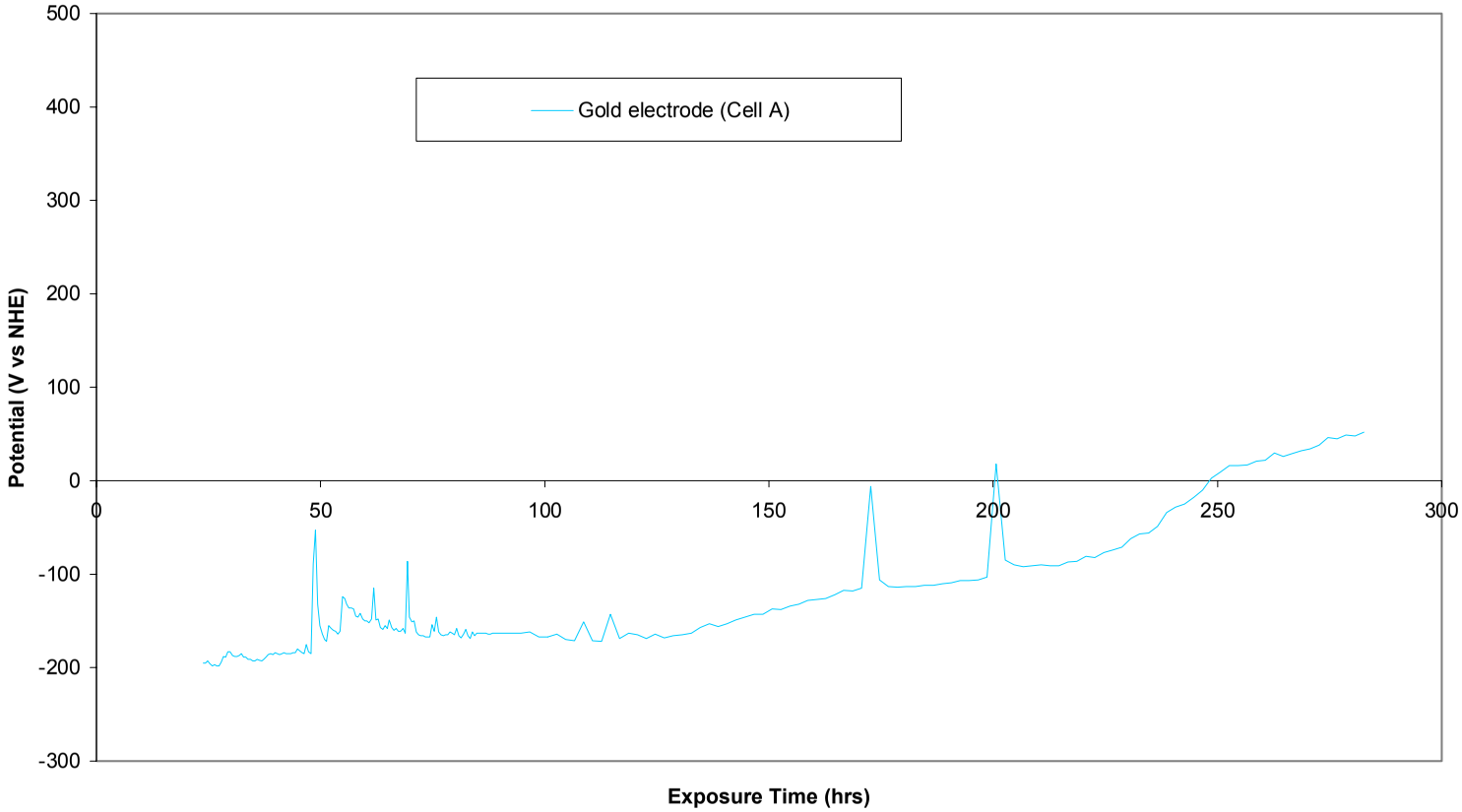

Figure 11. Potential of gold electrode in deaerated bentonite-equilibrated groundwater at 50ºC (Test 2, Cell A).

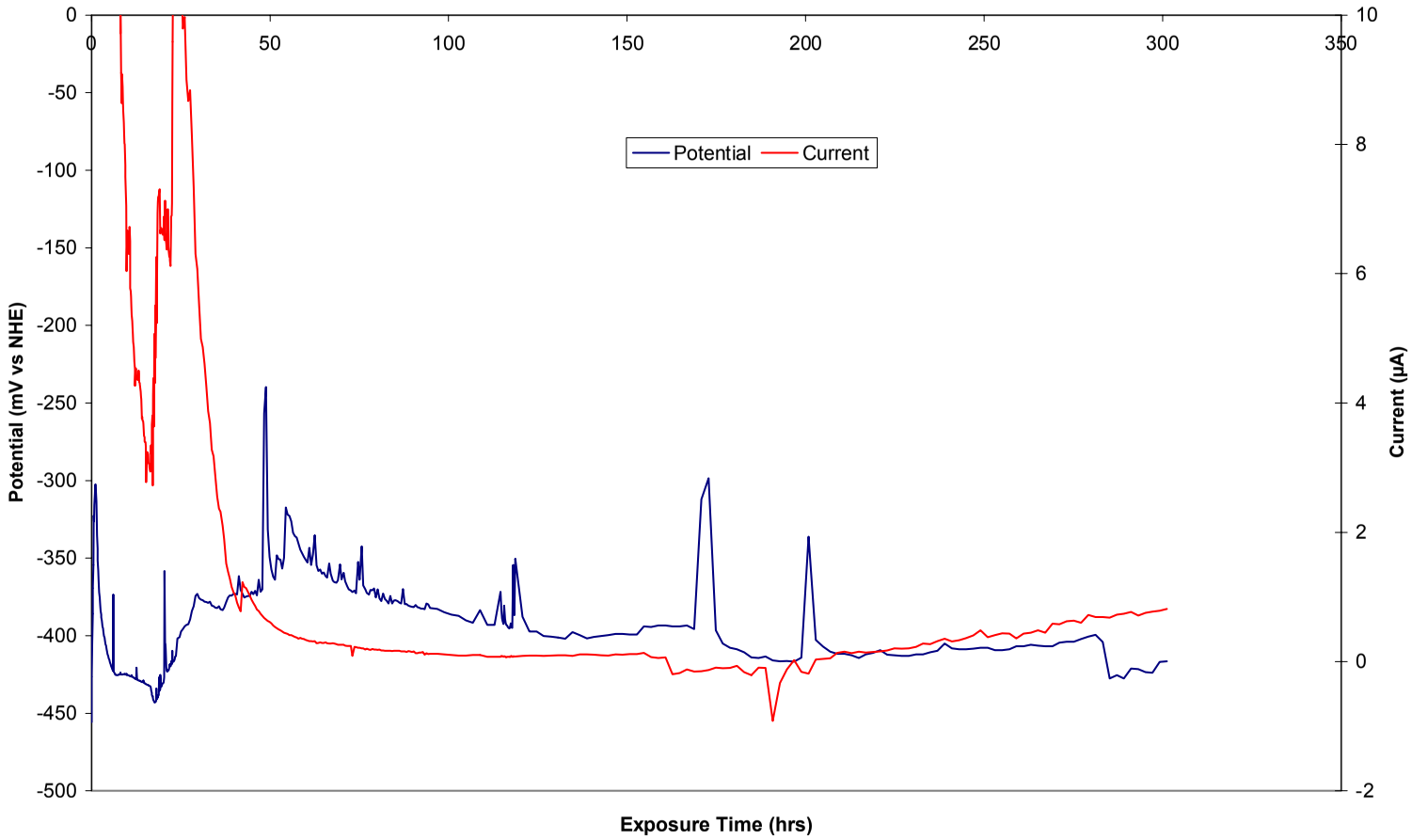

Figure 12. Currents passing between permanently coupled cast iron and copper electrodes in deaerated bentonite-equilibrated groundwater at 50° C, and potential of coupled electrodes (Test 2, Cell A).

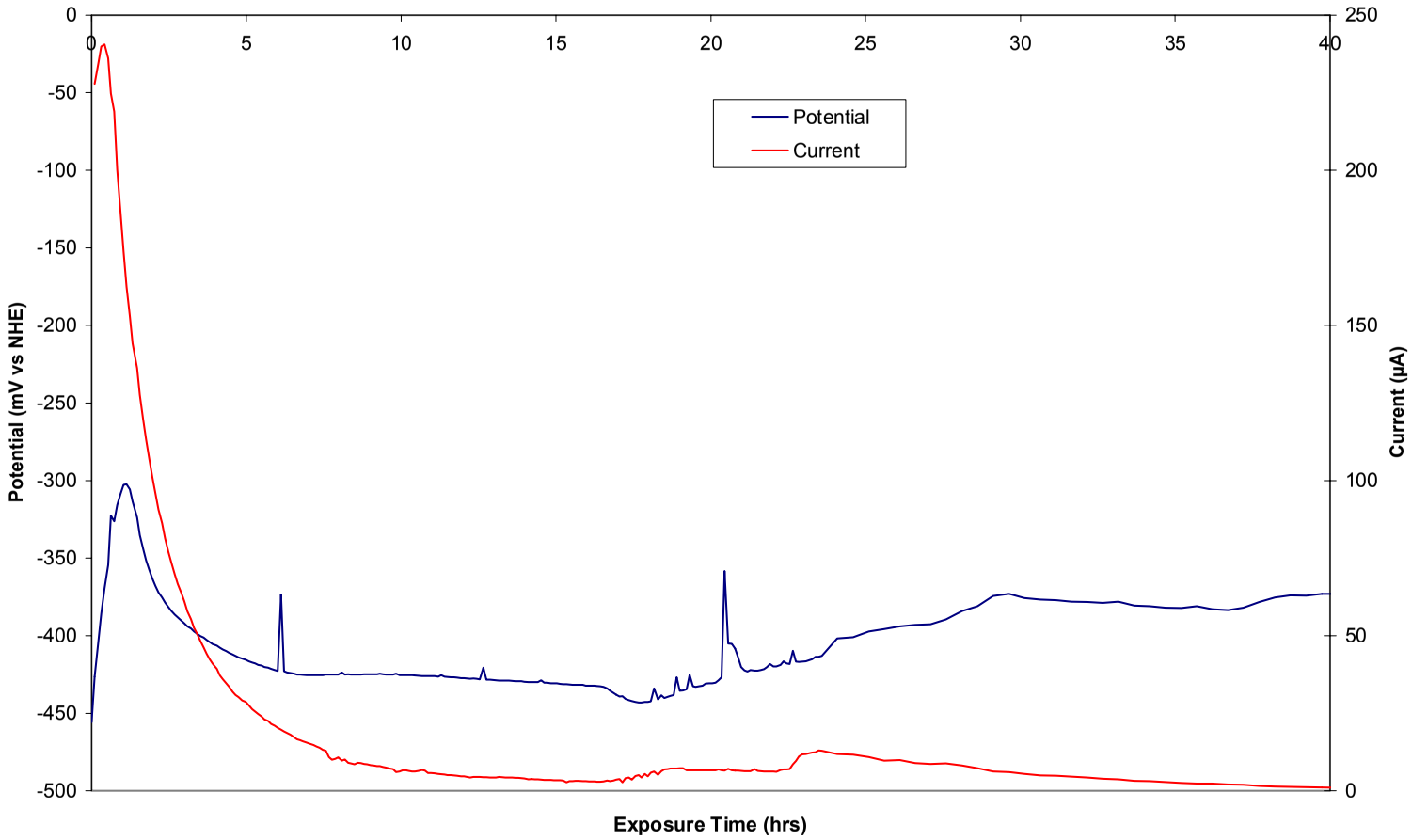

Figure 13. Currents passing between permanently coupled cast iron and copper electrodes in deaerated bentonite-equilibrated groundwater at 50° C, and potential of coupled electrodes (Test 2, Cell A) – initial response.

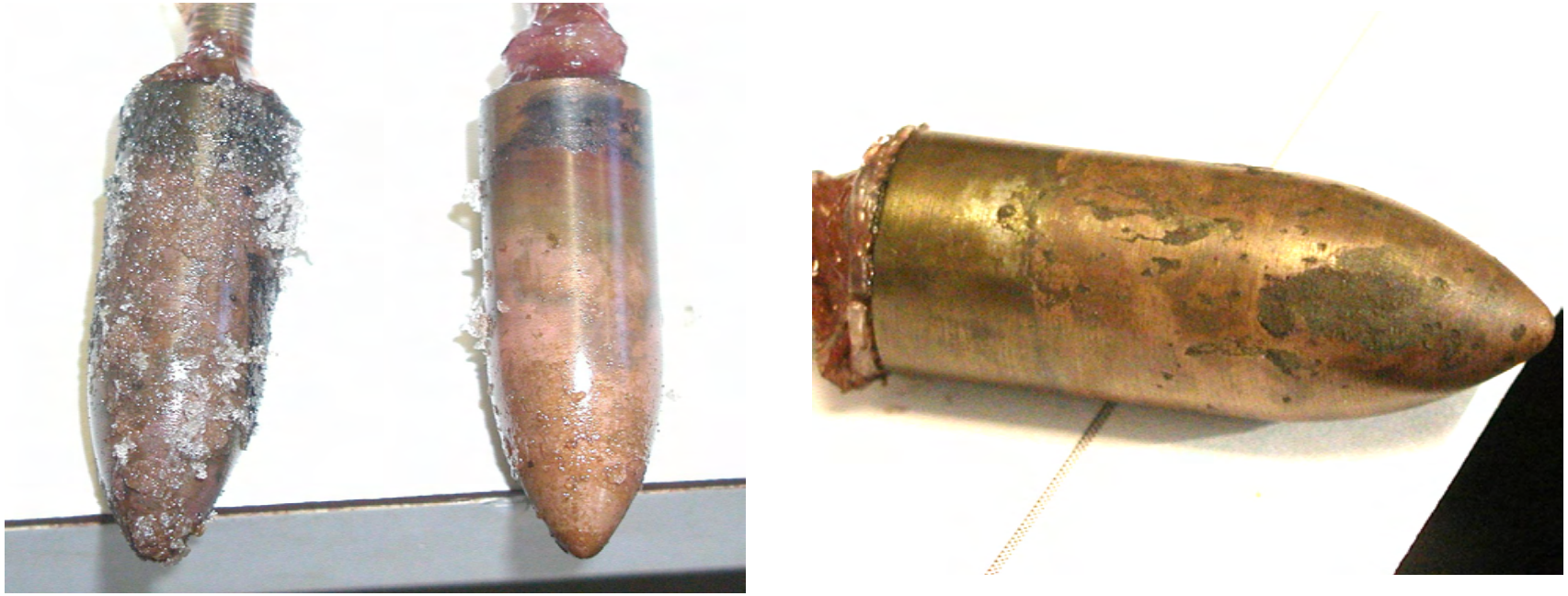

Figure 14. Specimens at the end of Test 2 (deaerated bentonite-equilibrated groundwater at 50º C); left: before washing, right: after washing. Note the copper colouration of the iron specimen on the right.

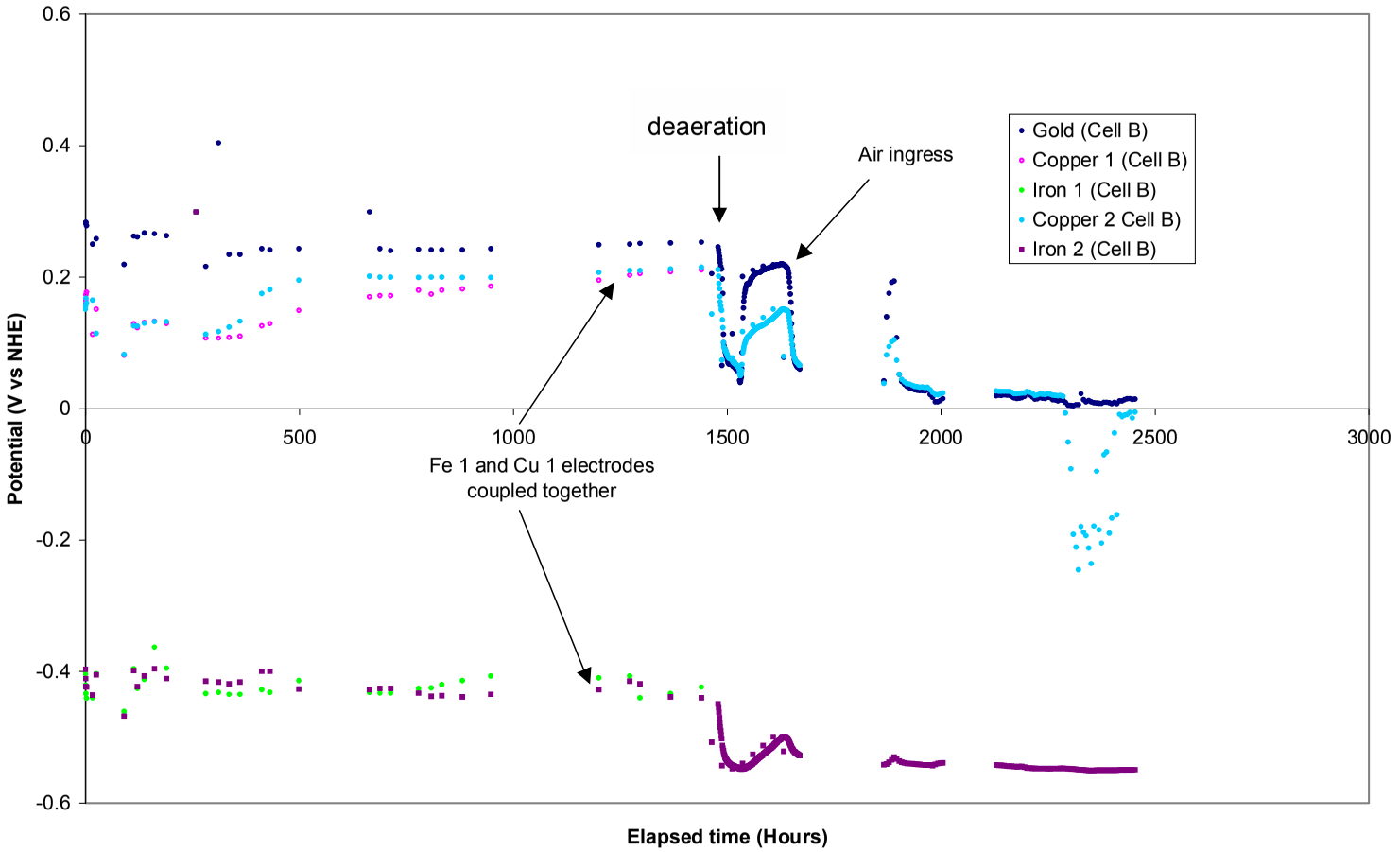

Figure 15. Potential of electrodes in bentonite-equilibrated groundwater at 50ºC, aerated then deaerated (Test 3).

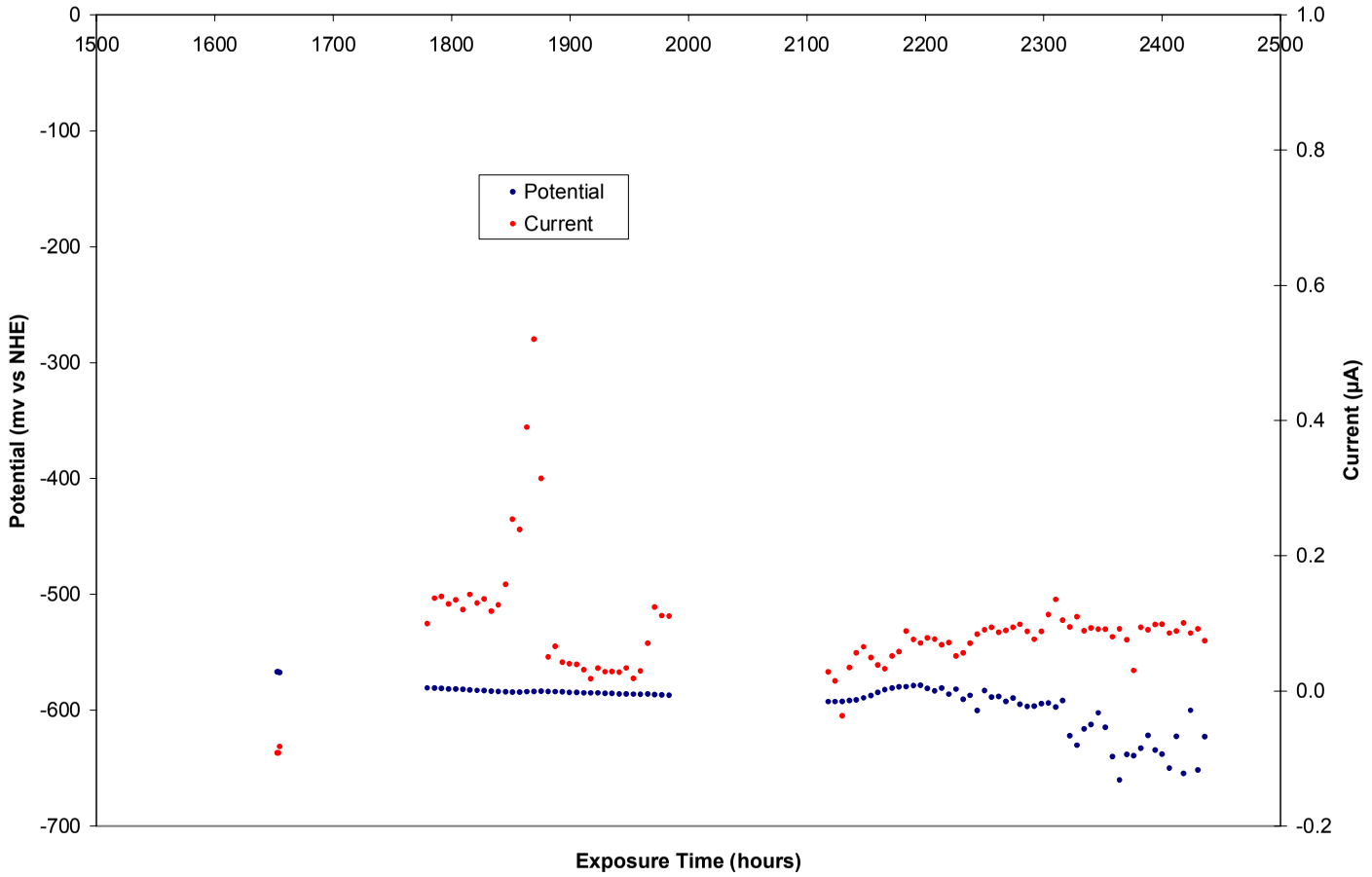

Figure 16. Currents passing between permanently coupled cast iron and copper electrodes in deaerated bentonite-equilibrated groundwater at 50°C and potential of coupled electrodes (Test 3).

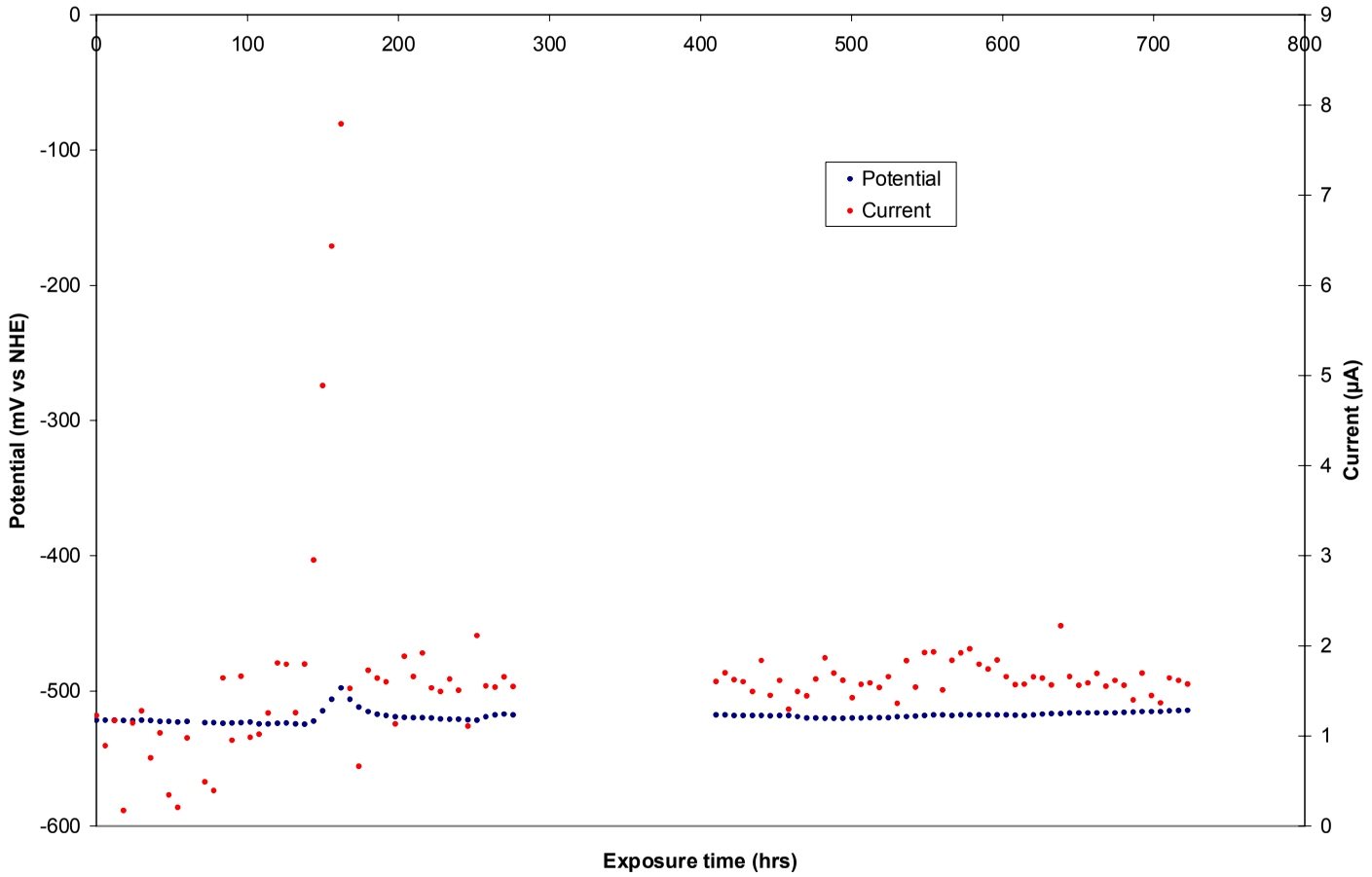

Figure 17. Currents passing between cast iron and copper electrodes in bentonite-equilibrated groundwater at 50ºC, aerated then deaerated, and potential of coupled electrodes (Test 3, Cell B). The electrodes were coupled after deaeration had started.

Figure 18. Specimens at the end of Test 3 (bentonite-equilibrated groundwater at 50ºC, aerated then deaerated, left Cell B, middle Cell A, right Cell A)

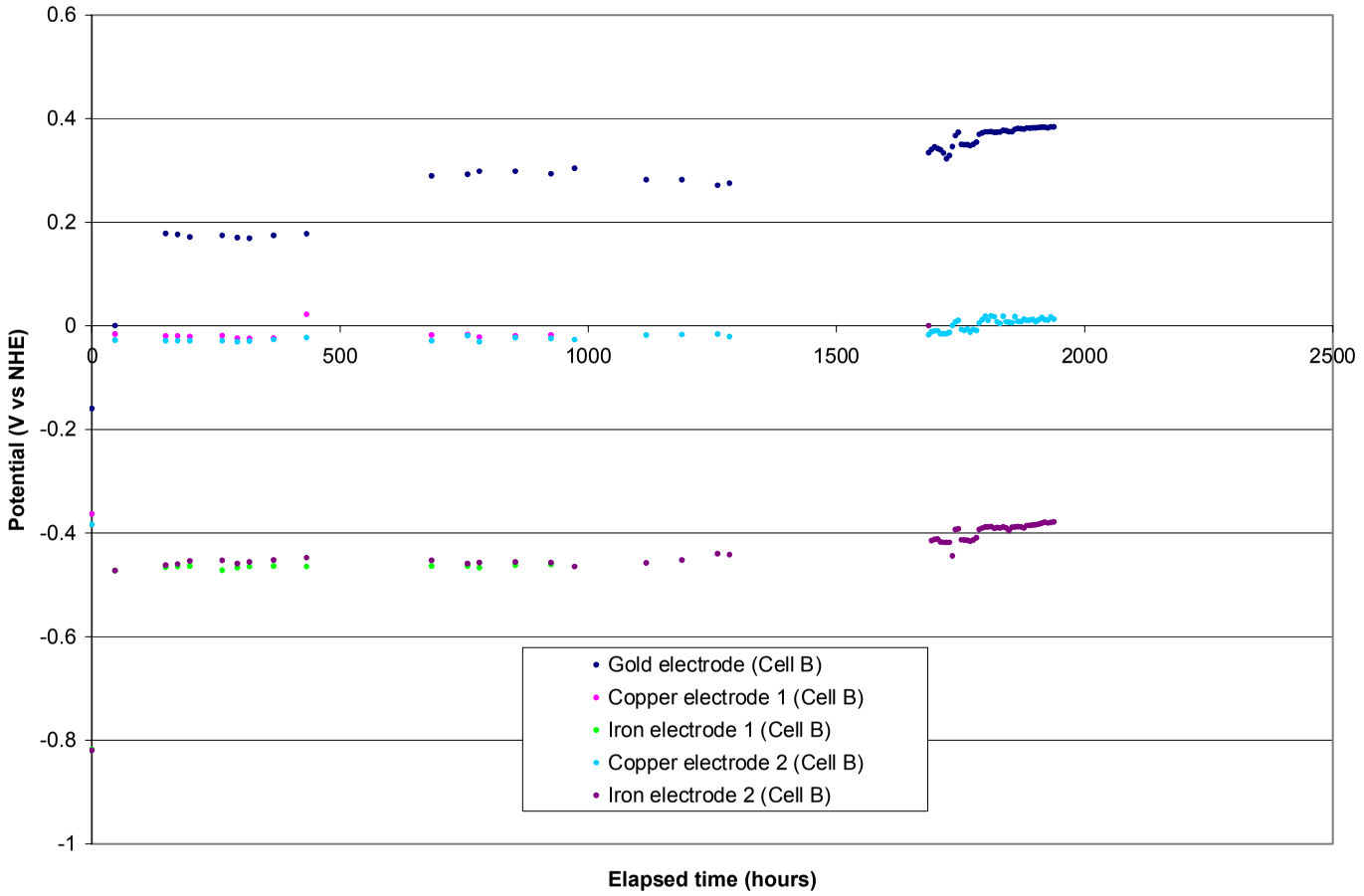

Figure 19. Potential of electrodes in deaerated bentonite-slurry at 50ºC (Test 4, Cell B).

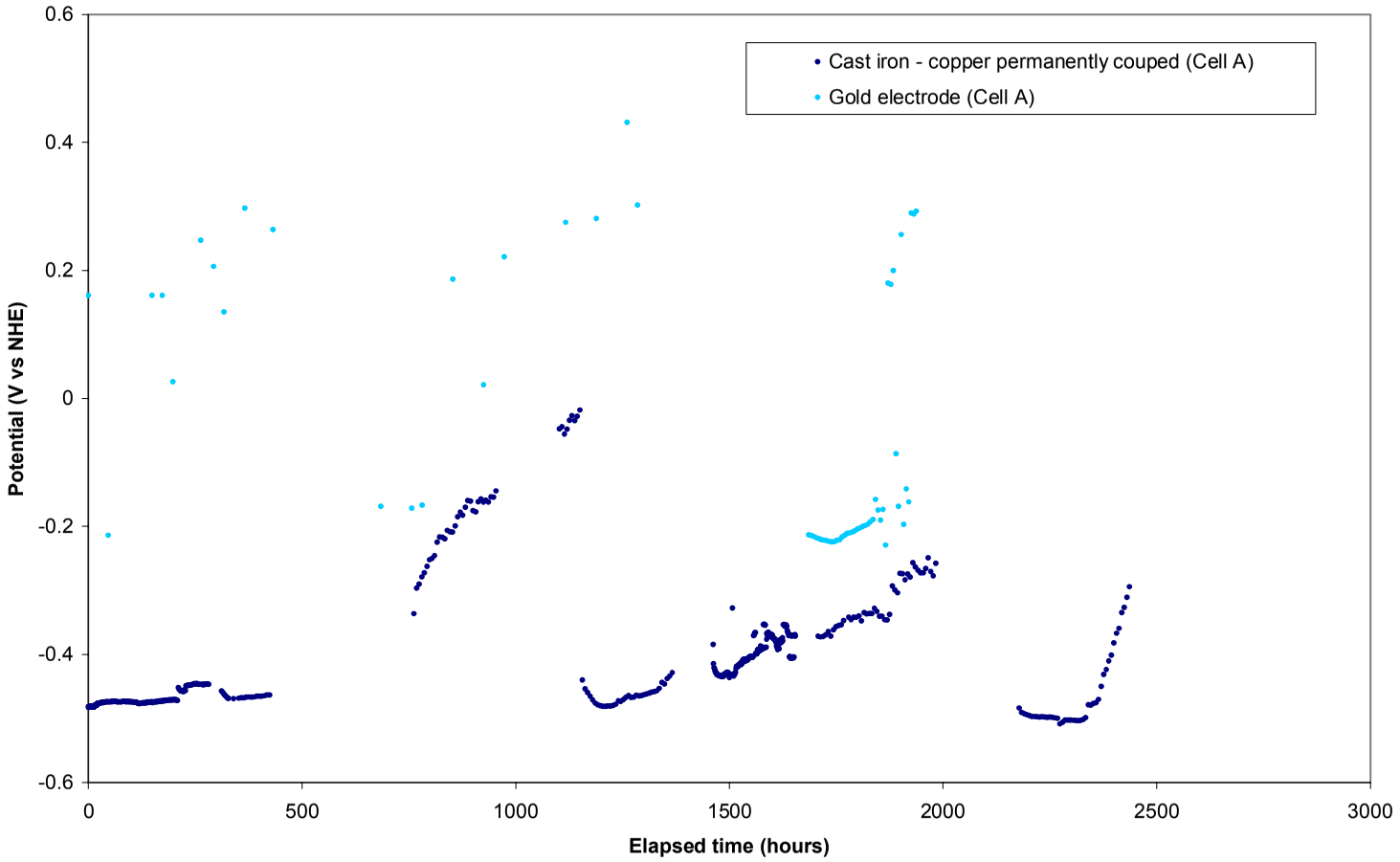

Figure 20 . Potential of electrodes in deaerated bentonite-slurry at 50ºC (Test 4, Cell A).

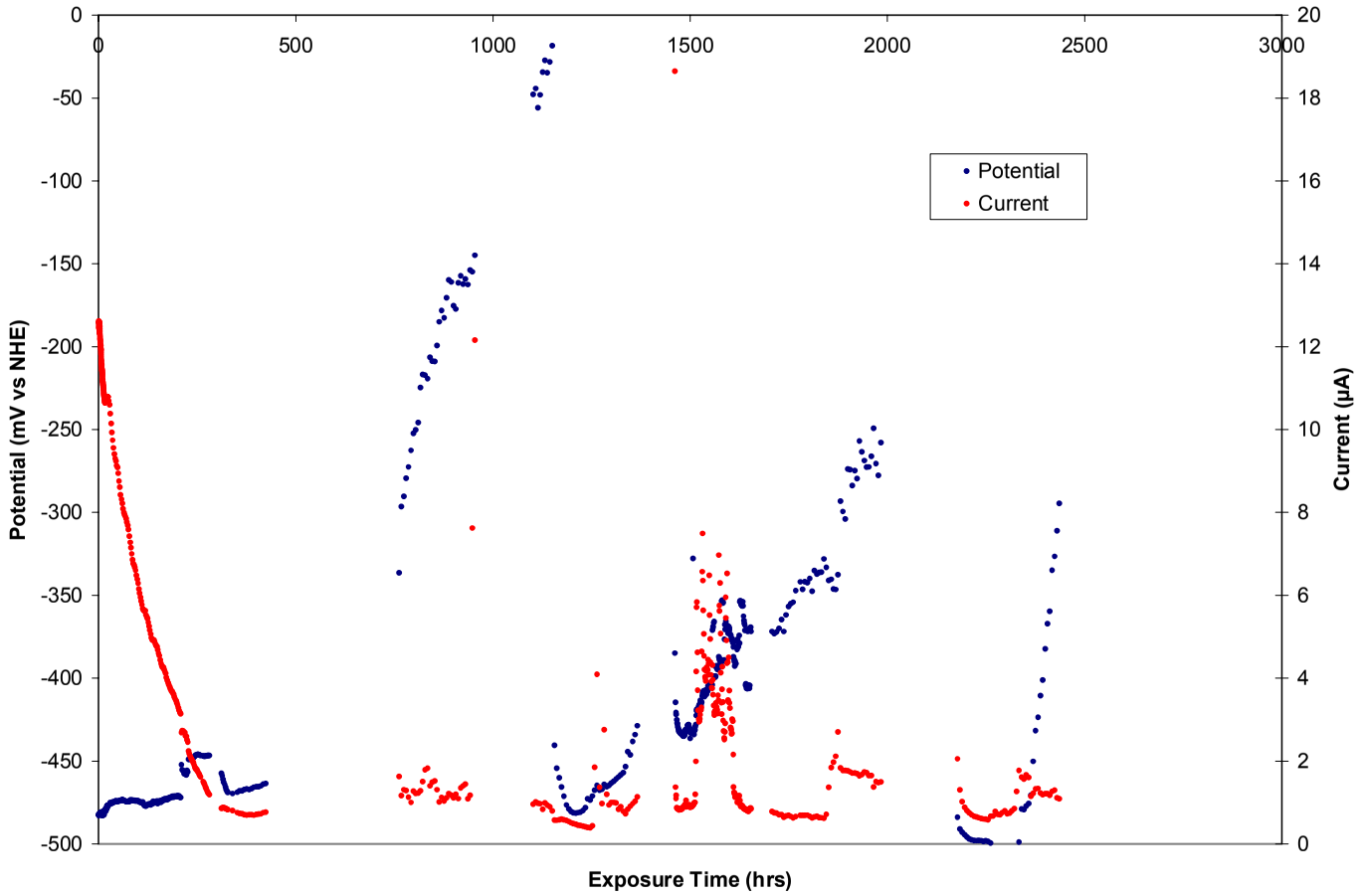

Figure 21. Currents passing between permanently coupled cast iron and copper electrodes in deaerated bentonite slurry at 50° C, and potential of coupled electrodes (Test 4).

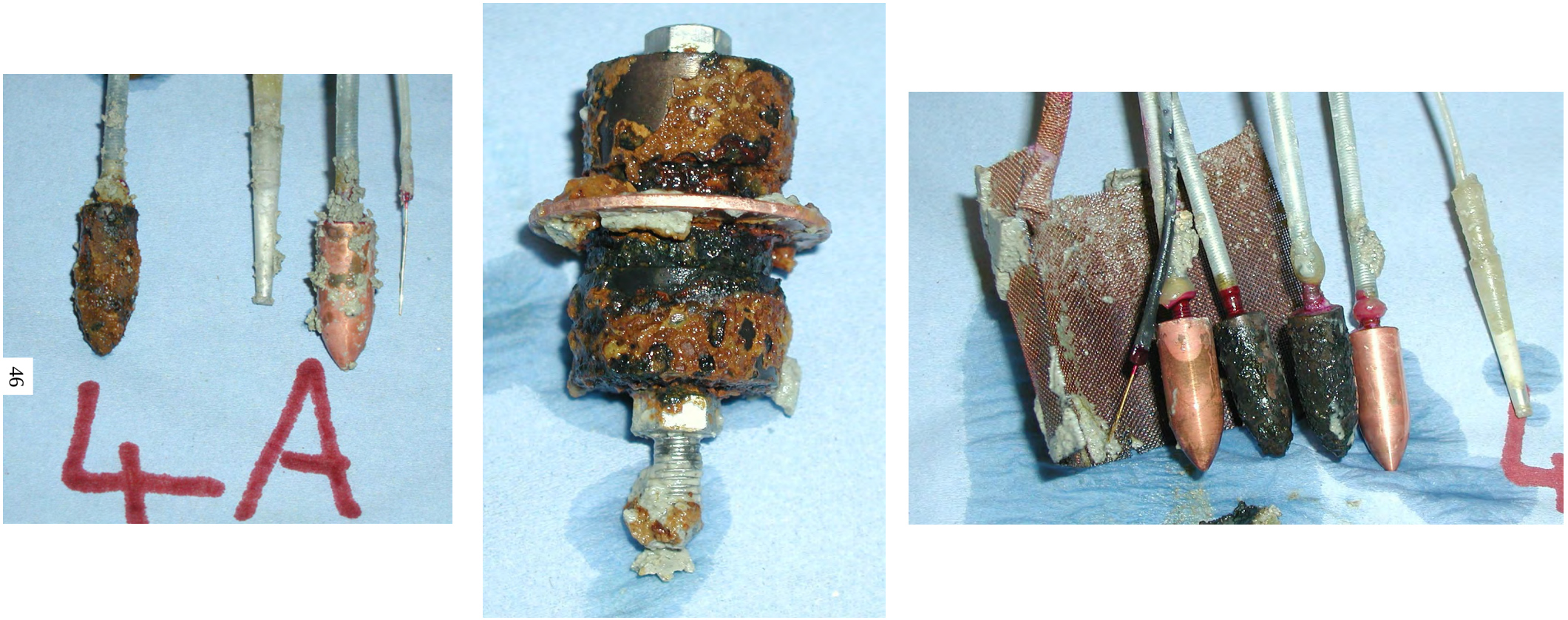

Figure 22. Specimens from Test 4 (deaerated bentonite slurry at 50° C, left Cell A, middle Cell A, right Cell B.

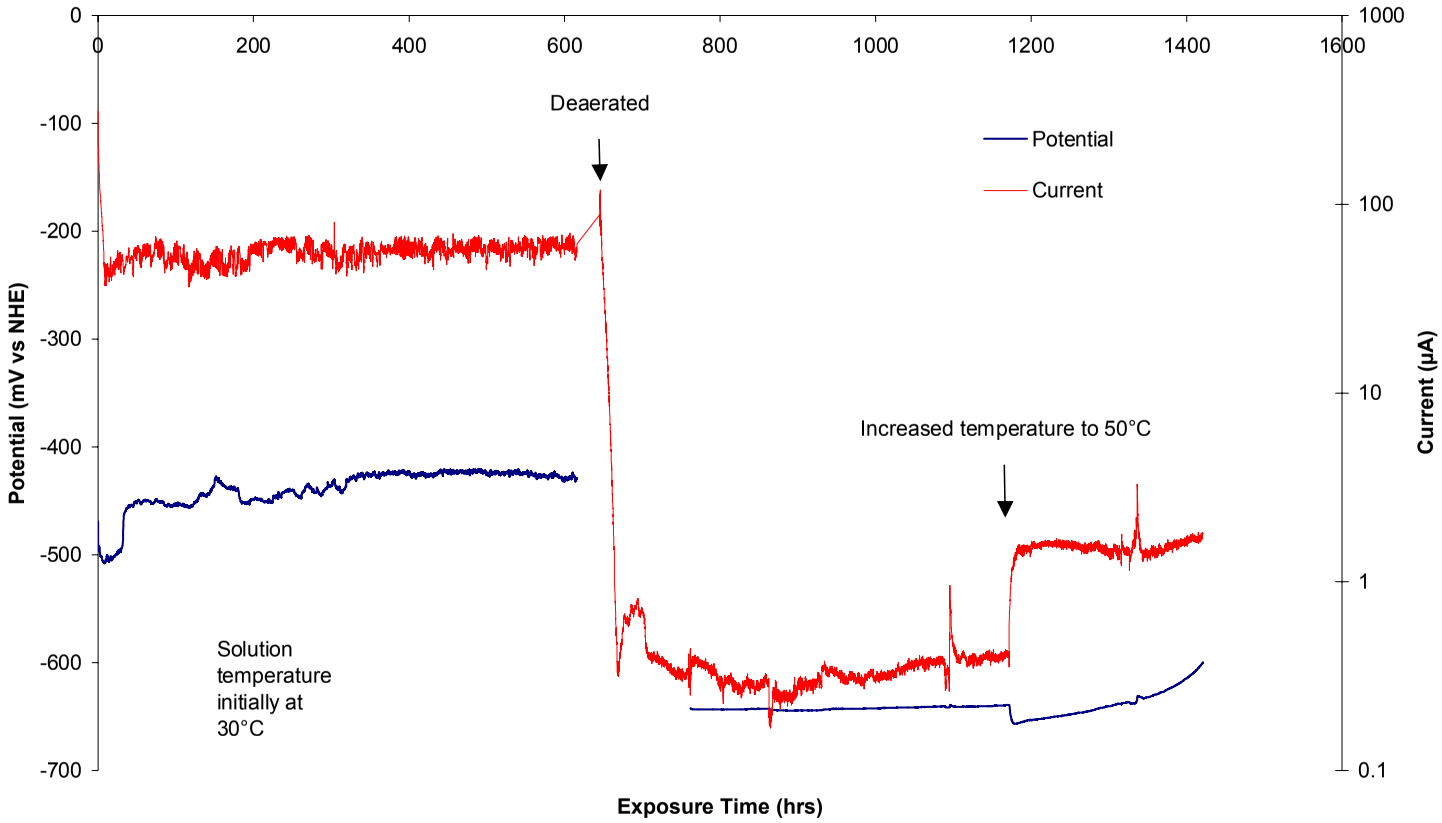

Figure 23. Currents passing between permanently coupled cast iron and copper electrodes in bentonite-equilibrated groundwater and potential of coupled electrodes (Test 9, Cell A). The solution was initially aerated then deaerated after 647 hours and the temperature was increased from 30 °C to 50 °C after 1172 hours. There was a temporary loss of potential data between 615 and 767 hours.

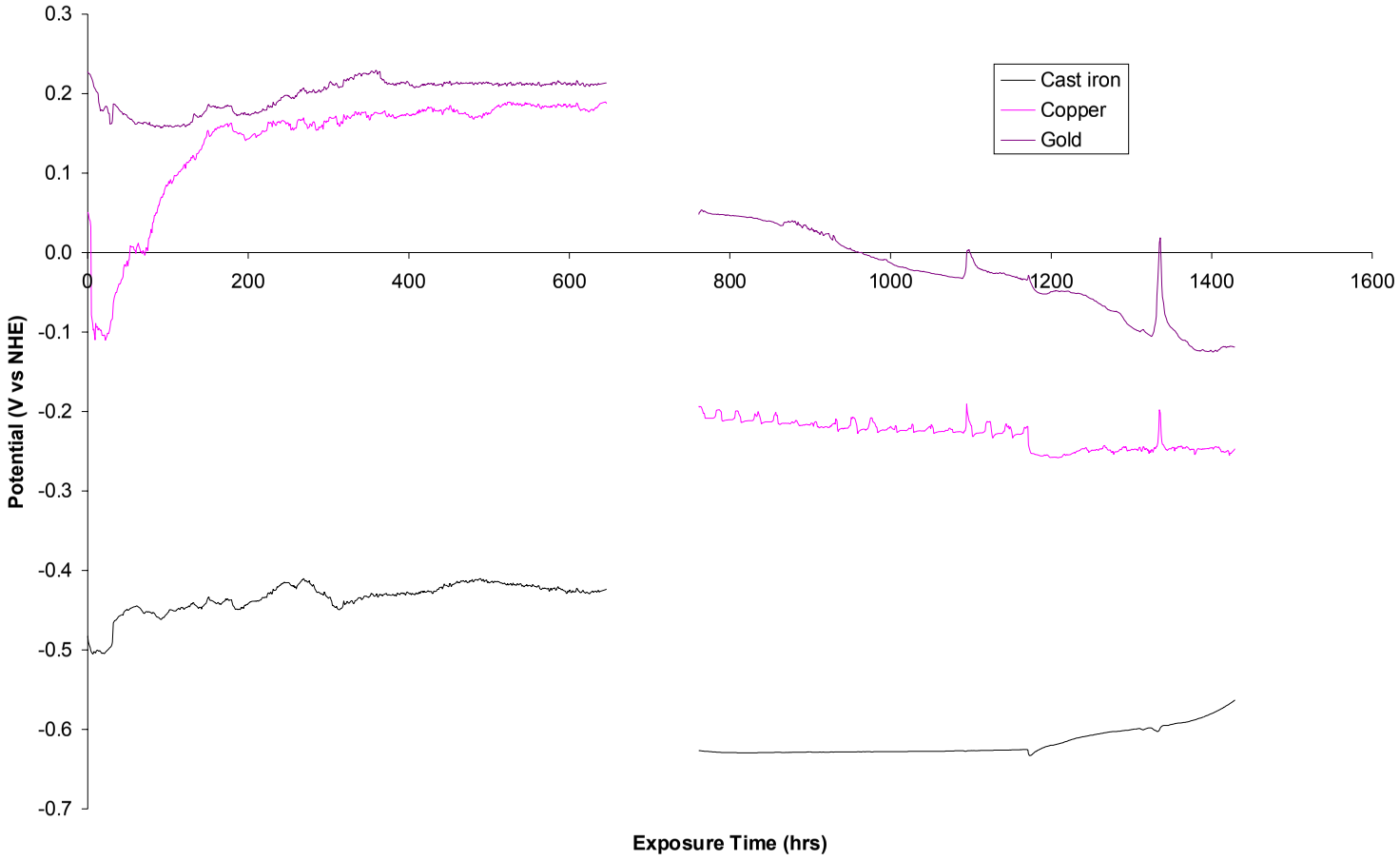

Figure 24. Potentials of electrodes in bentonite-equilibrated groundwater (Test 9, Cell A). The solution was initially aerated then deaerated after 647 hours and the temperature was increased from 30 °C to 50 °C after 1172 hours. There was a temporary loss of potential data between 615 and 767 hours.

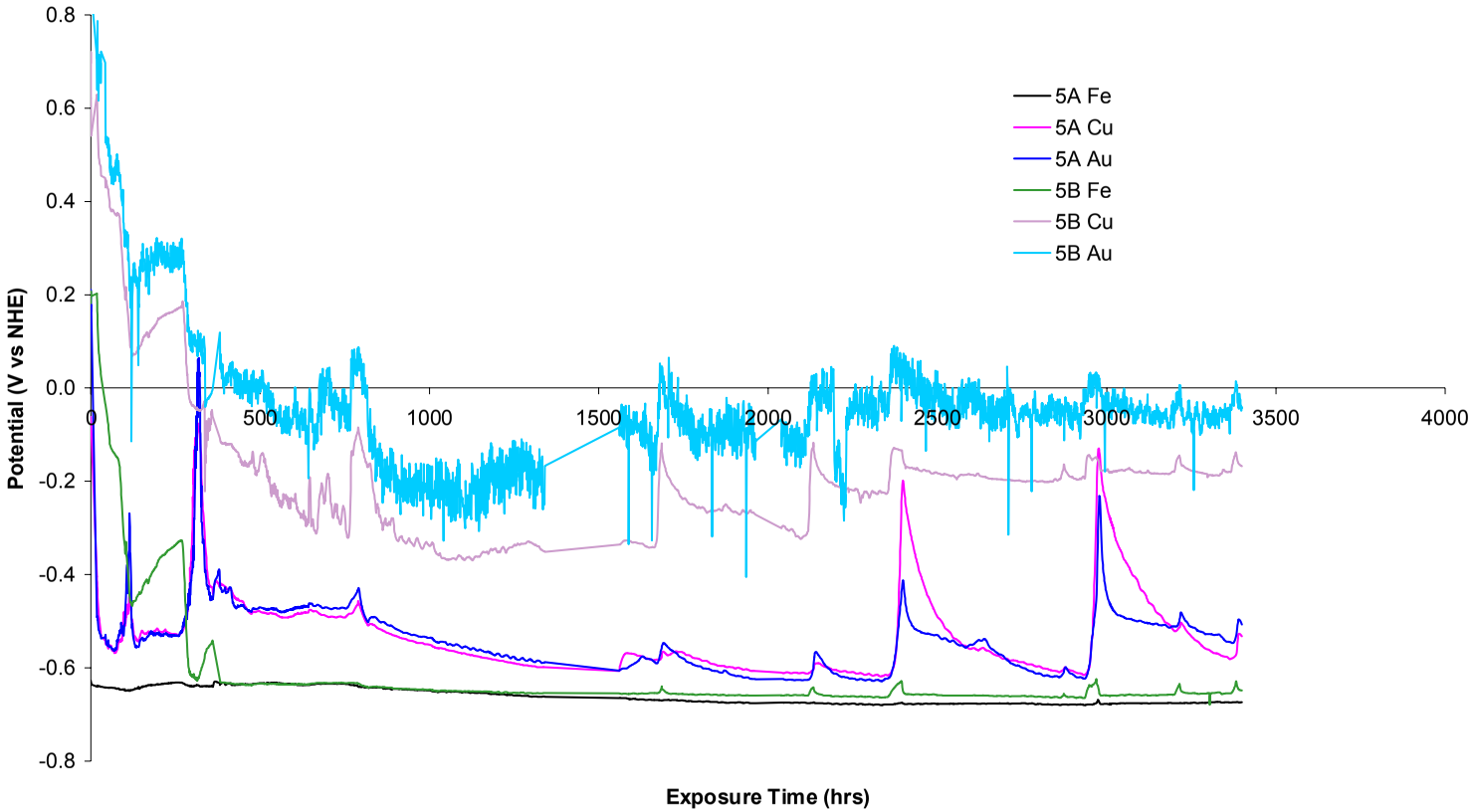

Figure 25. Potential of electrodes in deaerated Allard water at 30ºC (Test 5).

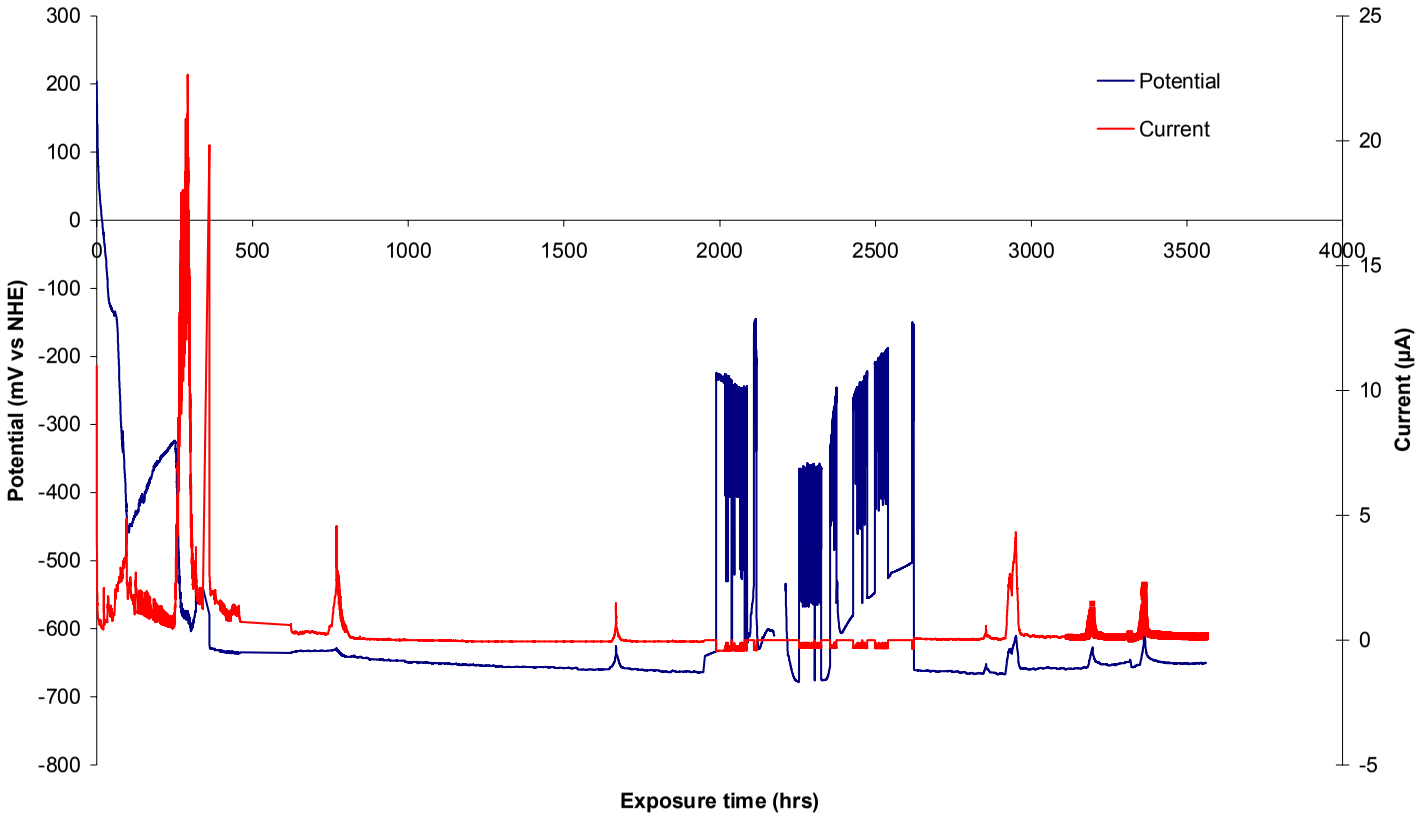

Figure 26. Currents passing between permanently coupled cast iron and copper electrodes in deaerated Allard water at 30º C, and potential of coupled electrodes (Test 5, Cell B).

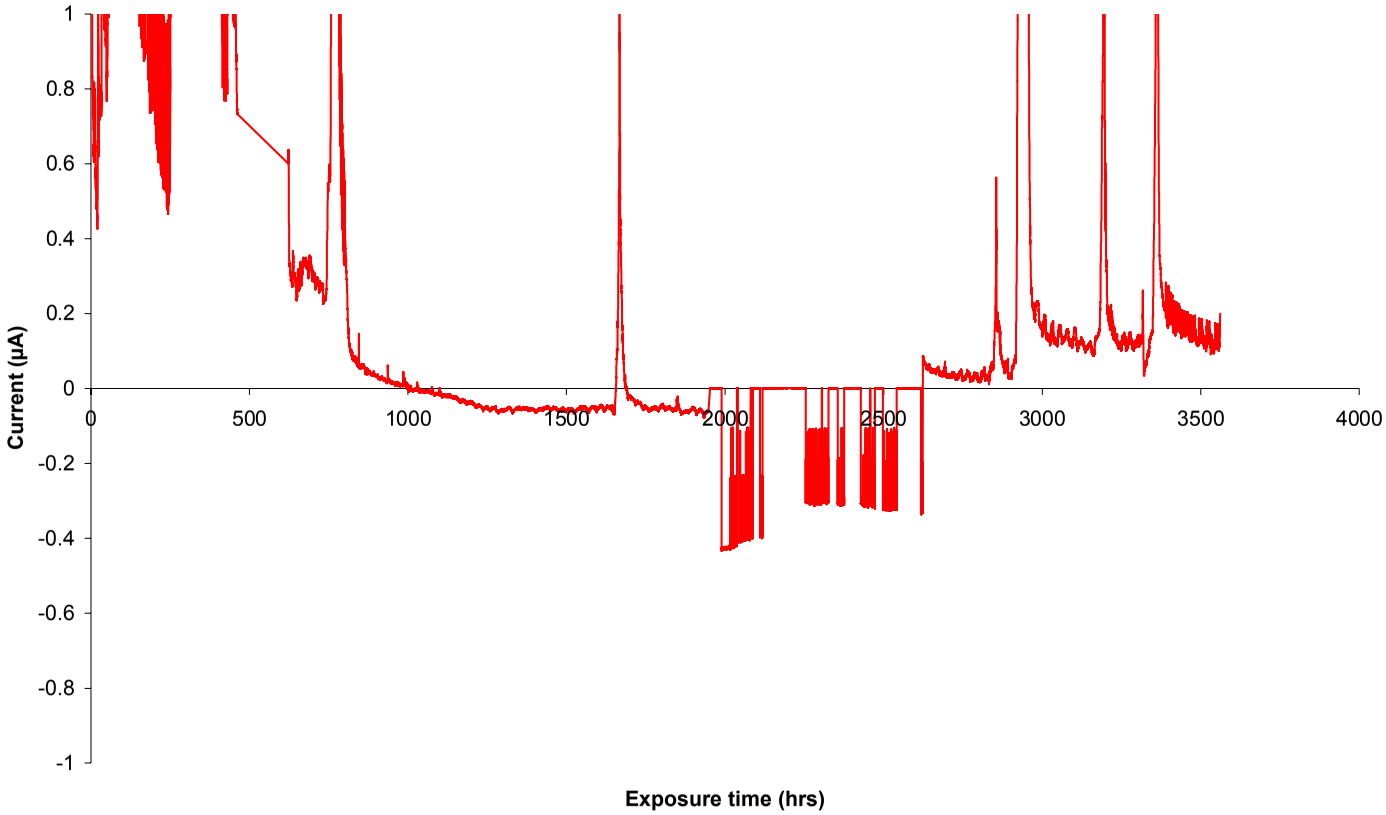

Figure 27. Currents passing between permanently coupled cast iron and copper electrodes in deaerated Allard water at 30º C (Test 5, Cell B) – expanded scale.

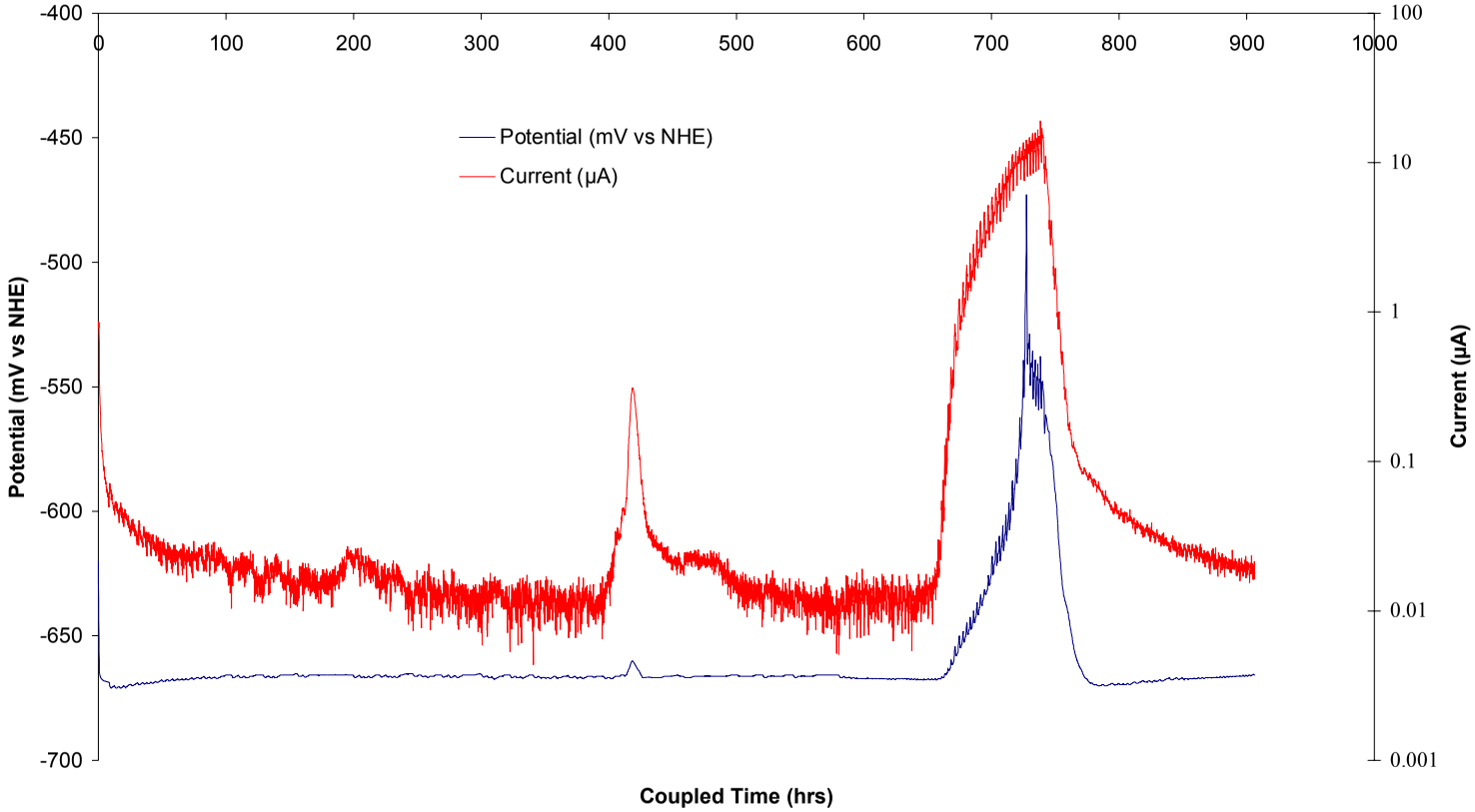

Figure 28. Currents passing between cast iron and copper electrodes in deaerated Allard water at 30° C, and potential of coupled electrodes (Test 5, Cell A) – electrodes coupled after 3410 hours of uncoupled corrosion.

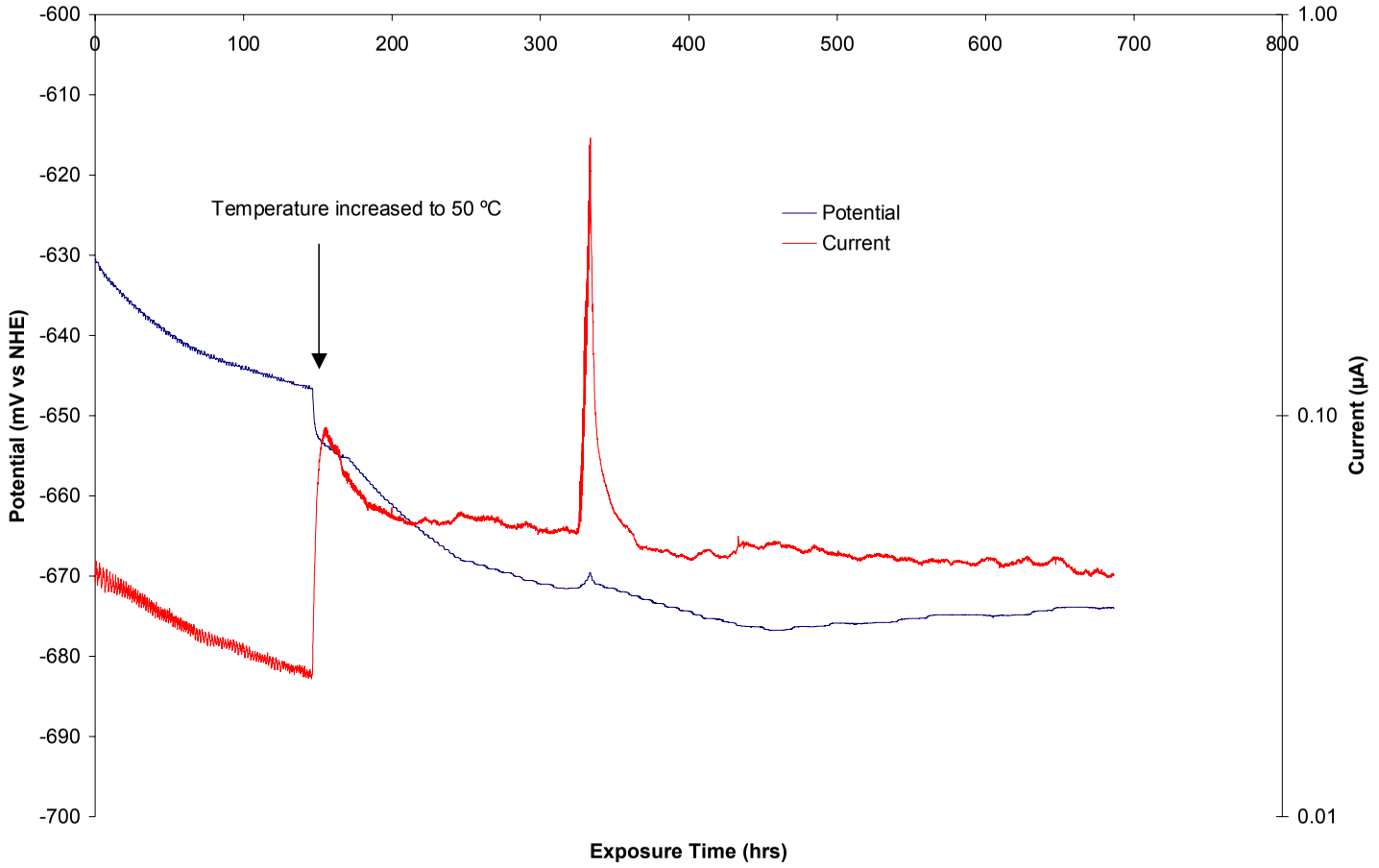

Figure 29. Currents passing between coupled cast iron and copper electrodes in deaerated Allard water at 30º C, and potential of coupled electrodes (Test 5, Cell A) - electrodes coupled after 3410 hours of uncoupled corrosion, showing effect of temperature increase.

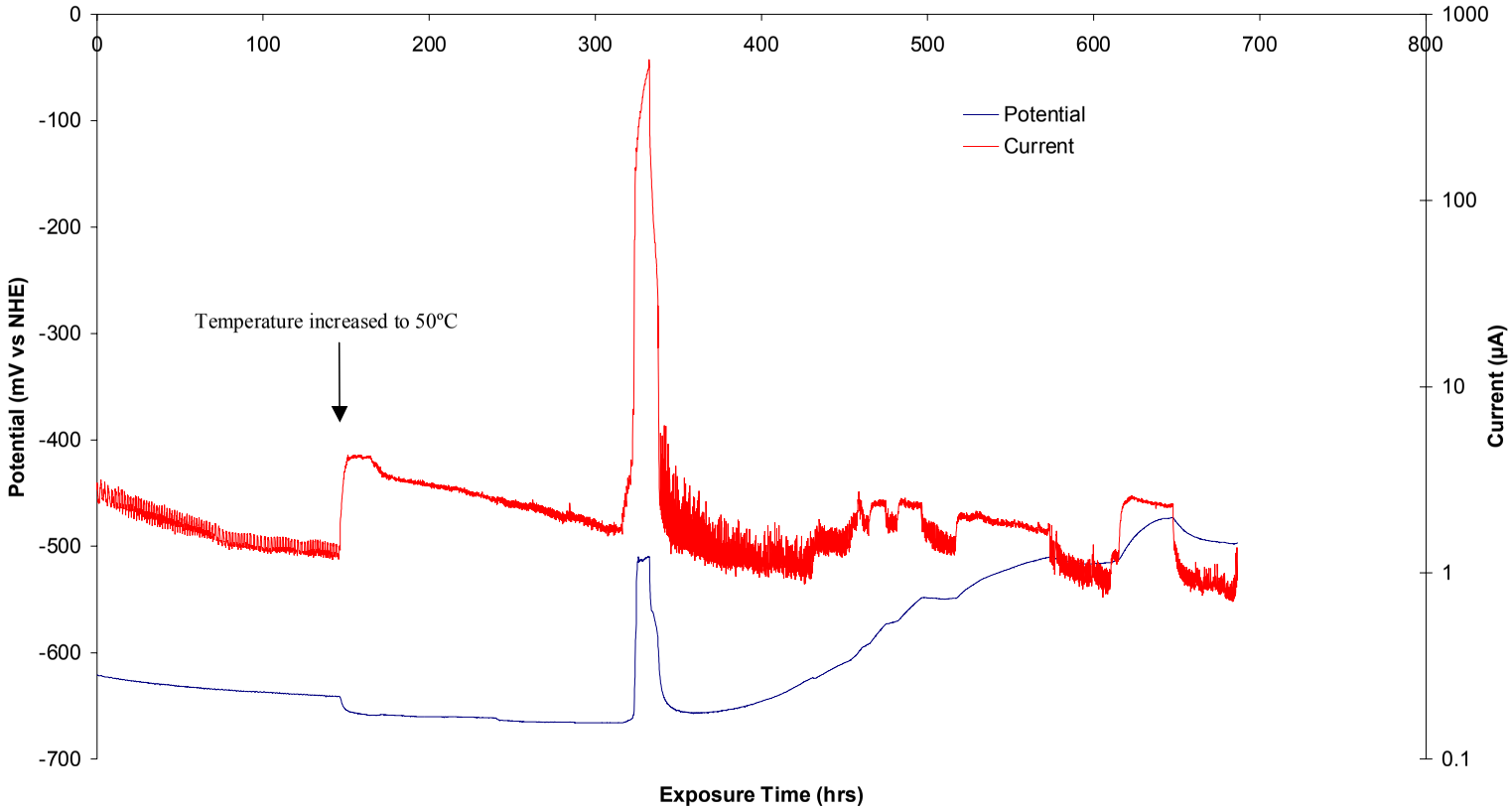

Figure 30. Currents passing between permanently coupled cast iron and copper electrodes in deaerated Allard water at 30º C, and potential of coupled electrodes (Test 5, Cell B), showing effect of temperature increase.

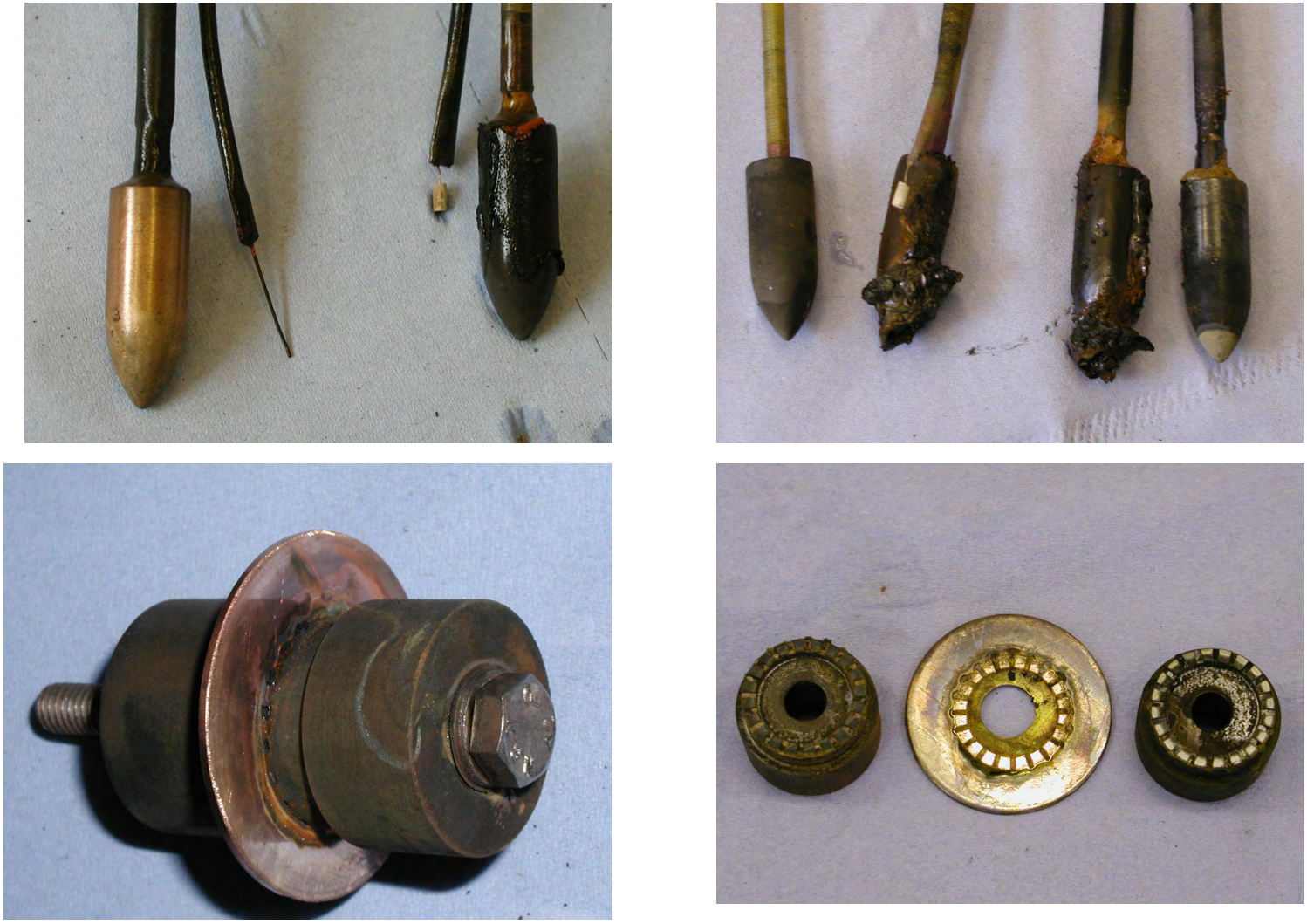

Figure 31. Specimens at end of Test 5 (deaerated Allard water at 30° C; top left Cell A, top right Cell B).

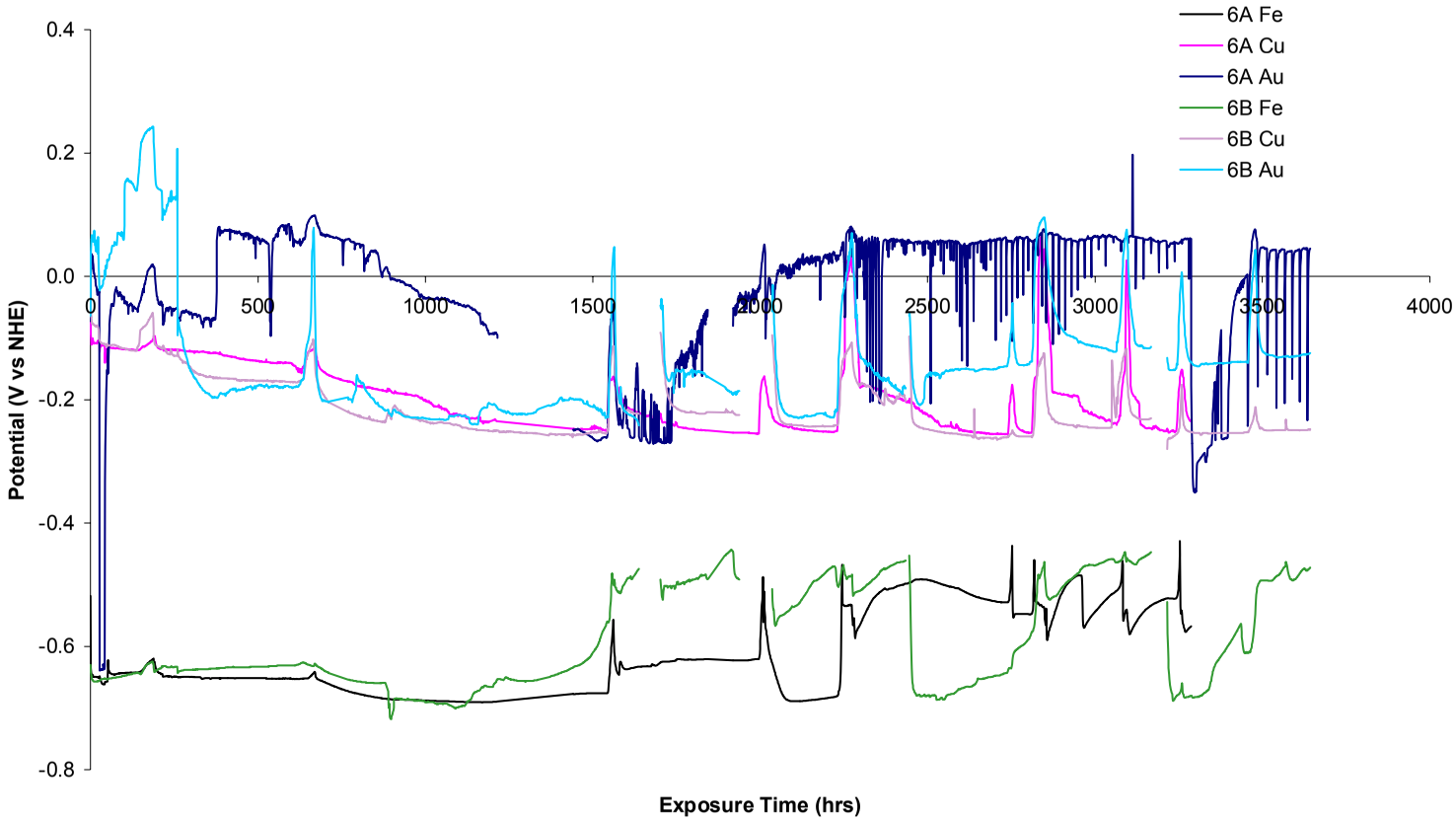

Figure 32. Potential of electrodes in deaerated Allard water at 50ºC (Test 6).

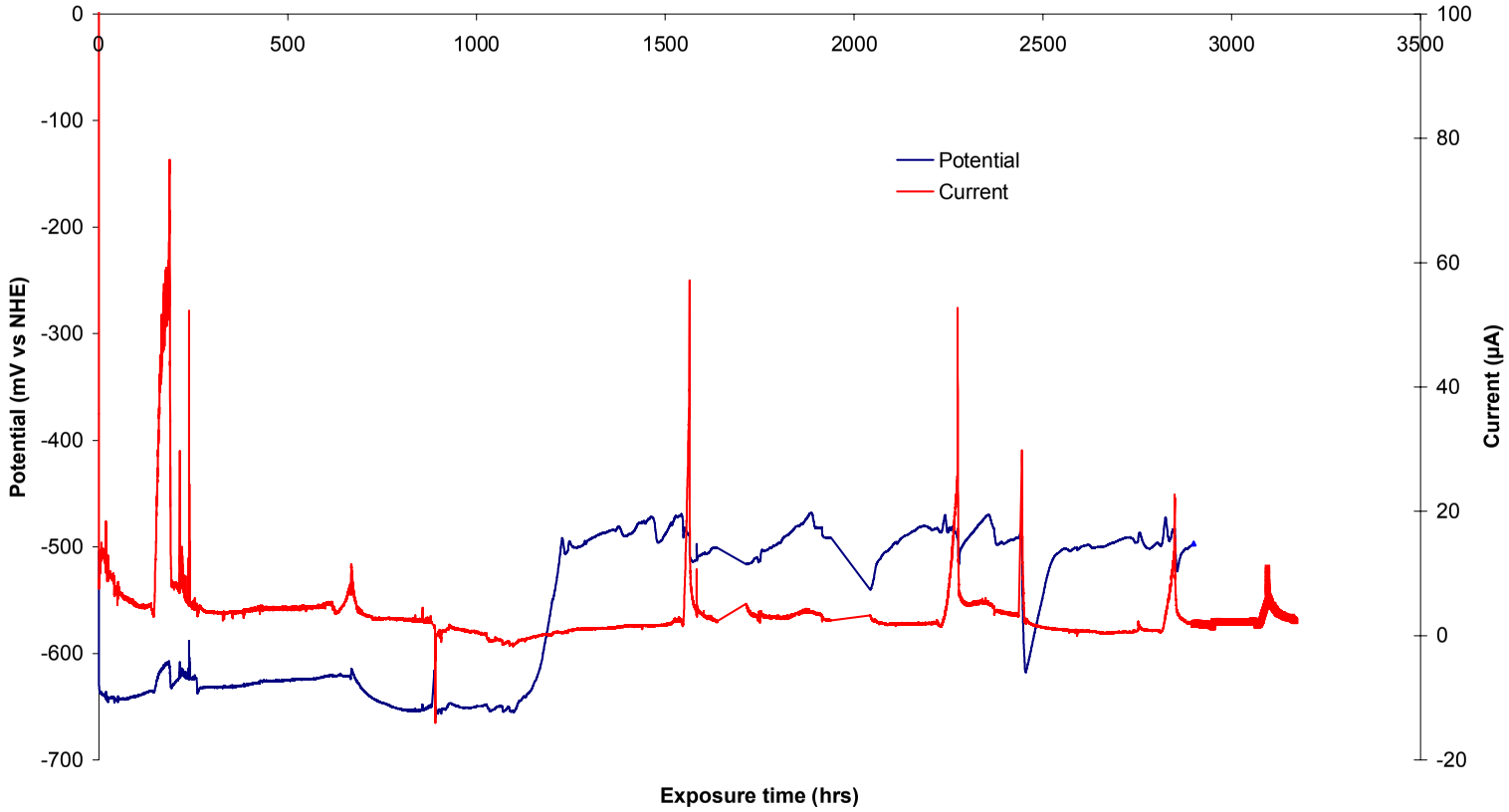

Figure 33. Currents passing between permanently coupled cast iron and copper electrodes in deaerated Allard water at 50°C, and potential of coupled electrodes (Test 6, Cell B).

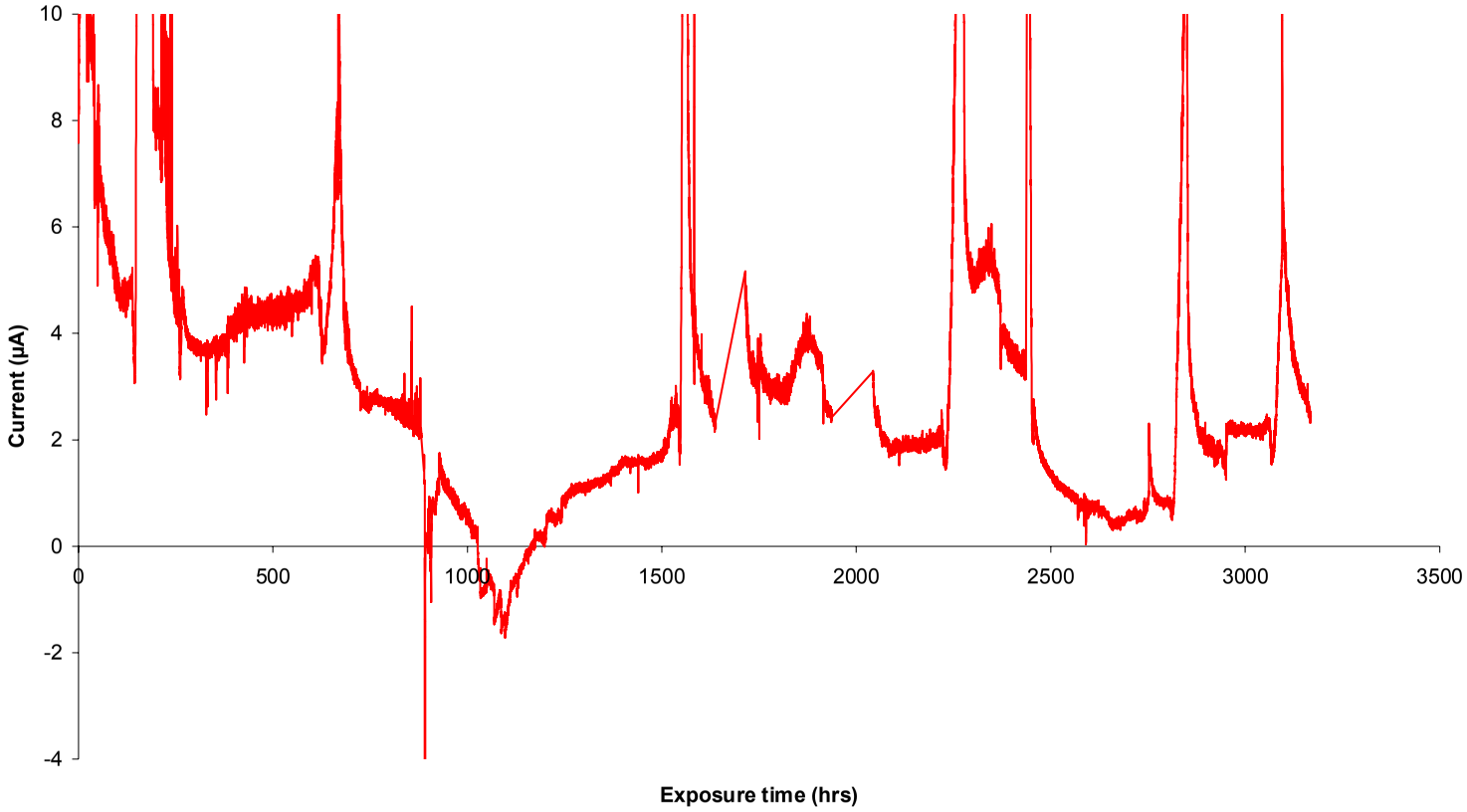

Figure 34. Currents passing between permanently coupled cast iron and copper electrodes in deaerated Allard water at 50ºC, and potential of coupled electrodes (Test 6, Cell B) – expanded scale.

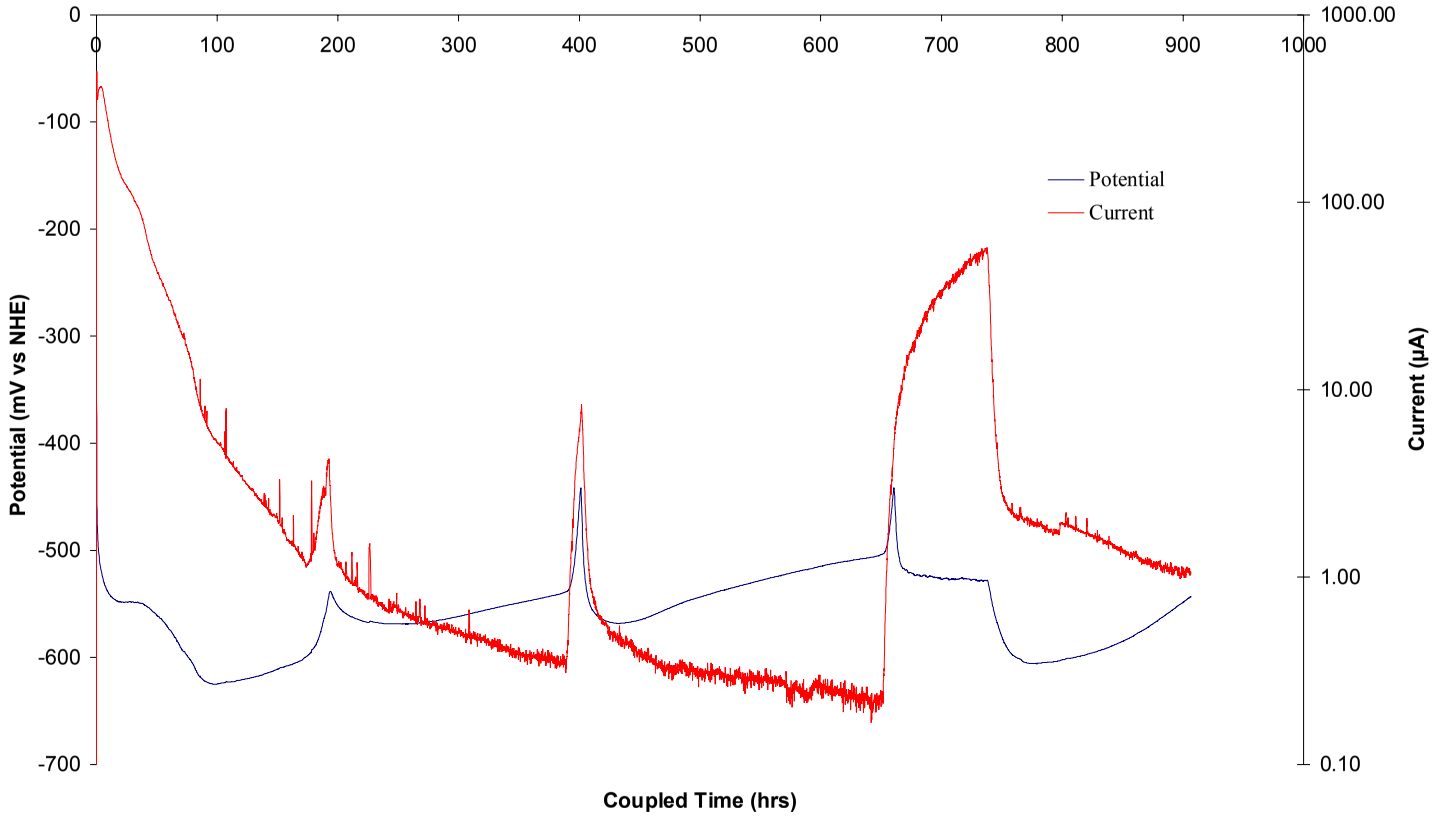

Figure 35. Currents passing between cast iron and copper electrodes in deaerated Allard water at 50ºC, and potential of coupled electrodes (Test 6, Cell A) – electrodes coupled after 3365 hours of uncoupled corrosion.

Figure 36. Specimens at end of Test 6 (deaerated Allard water at 50° C, left Cell A, right Cell B)

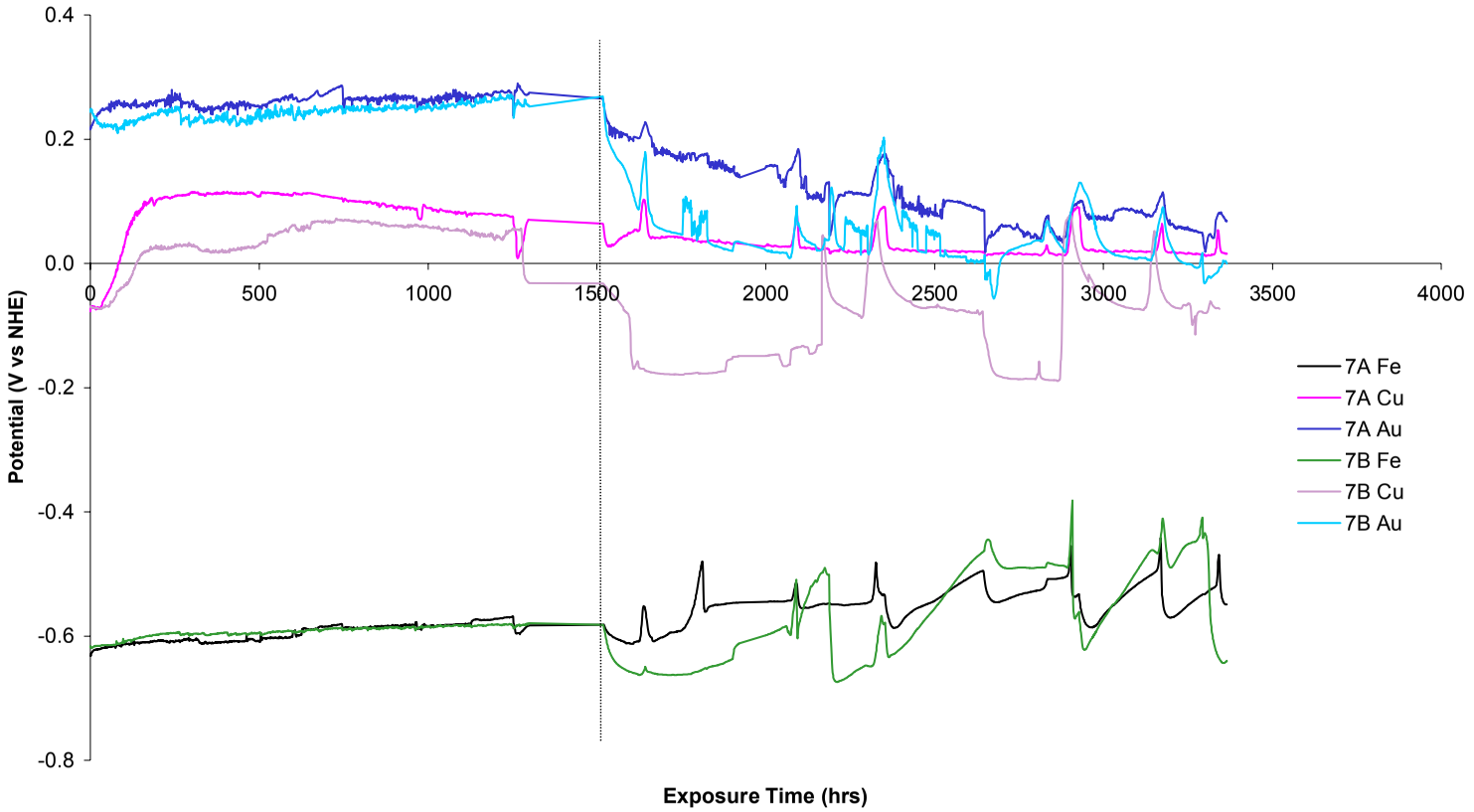

Figure 37. Potential of electrodes in Allard water at 50ºC - aerated initially then deaerated after 1500 hours (Test 7). The dotted line shows the point at which deaeration was started.

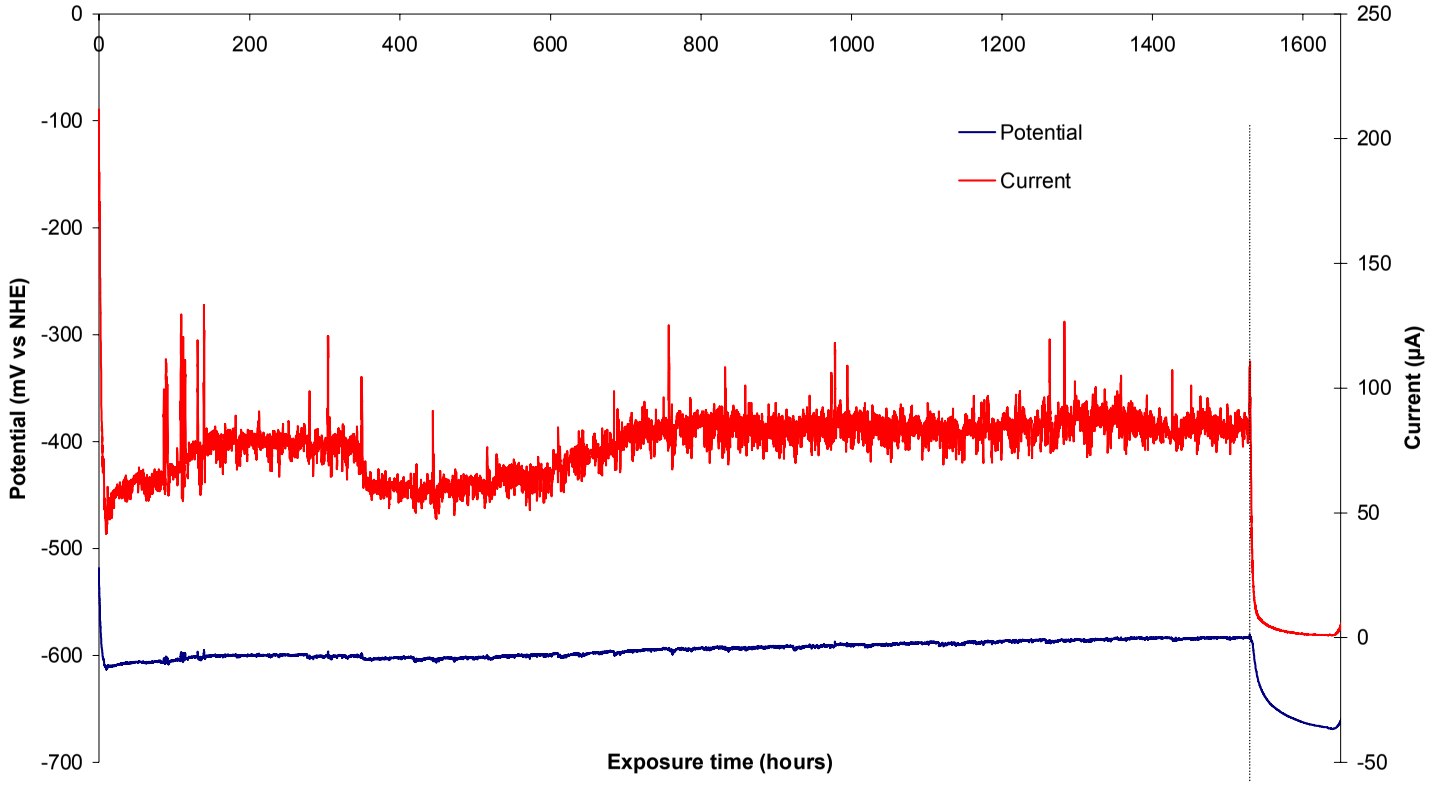

Figure 38. Currents passing between permanently coupled cast iron and copper electrodes in Allard water at 50ºC - aerated initially then deaerated after 1500 hours, and potential of coupled electrodes (Test 7, cell B). The dotted line indicates when deaeration was started.

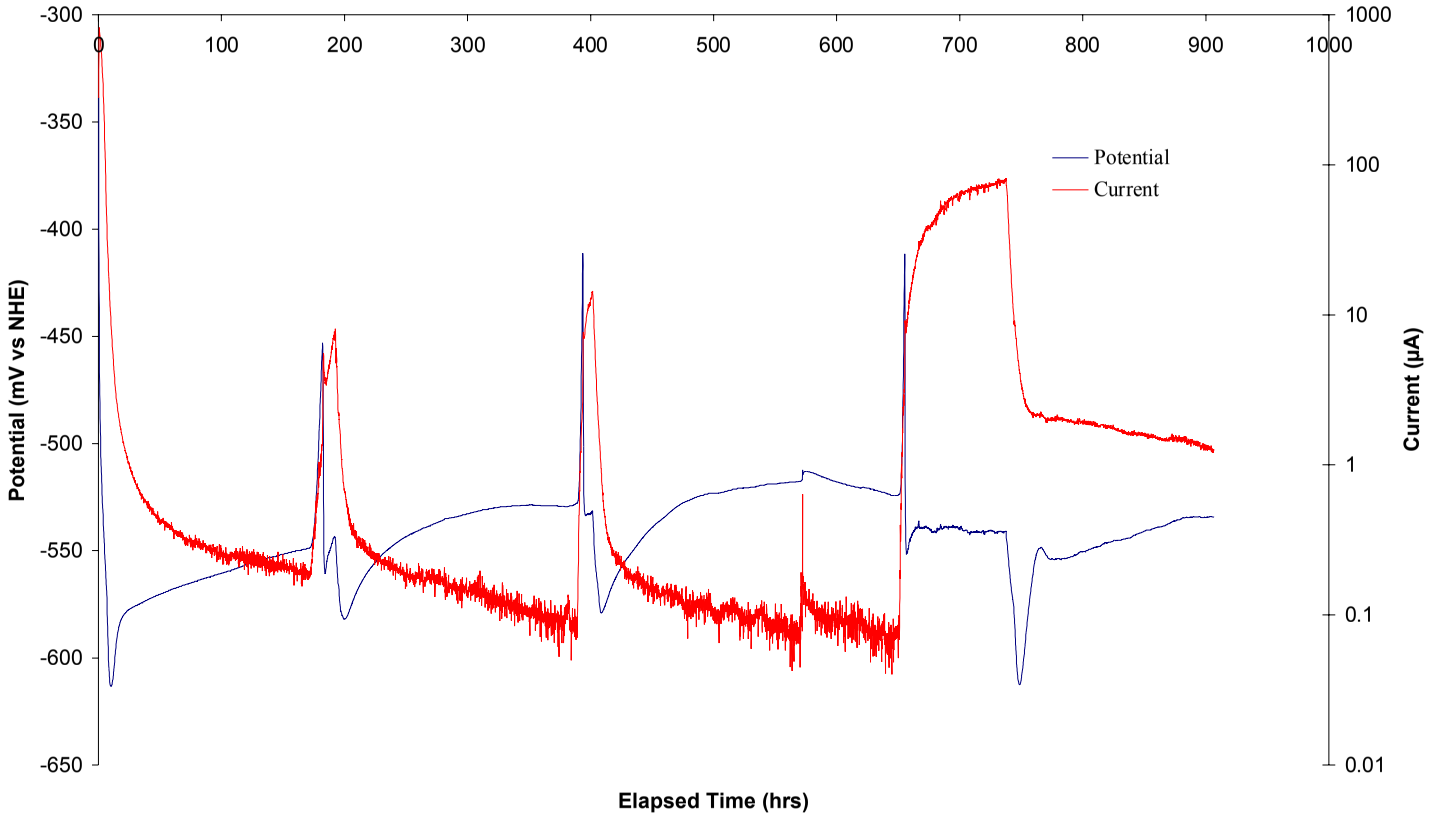

Figure 39. Currents passing between cast iron and copper electrodes in Allard water at 50ºC - aerated initially then deaerated after 1500 hours, and potential of coupled electrodes (Test 7, cell A). The electrodes were coupled after 3287 hours exposure to solution.

Figure 40. Specimens at end of Test 7 (initially aerated then deaerated, Allard water at 50° C).

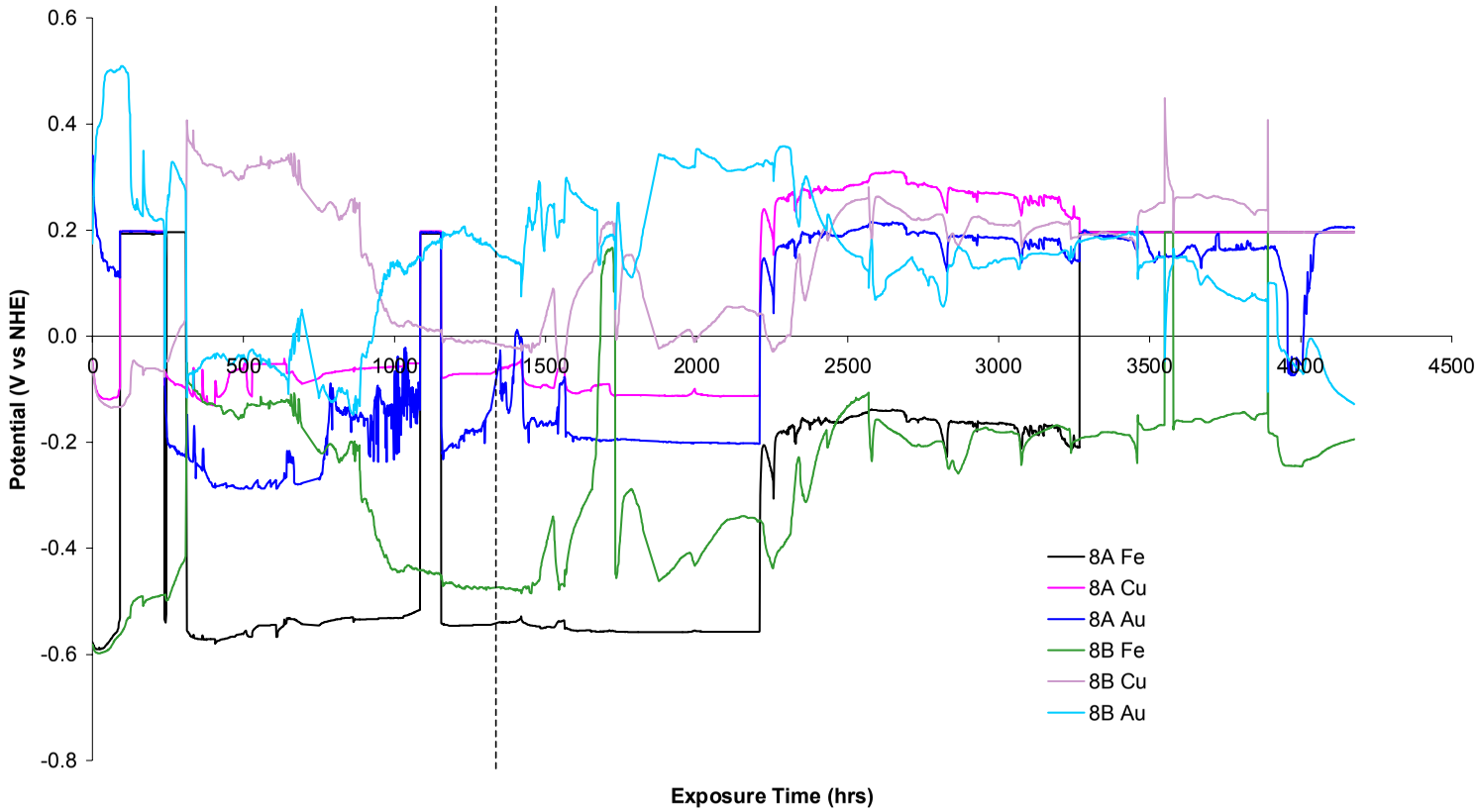

Figure 41. Potential of electrodes in deaerated bentonite slurry at 50ºC - aerated initially then deaerated (Test 8). The dotted line indicates when deaeration was commenced.

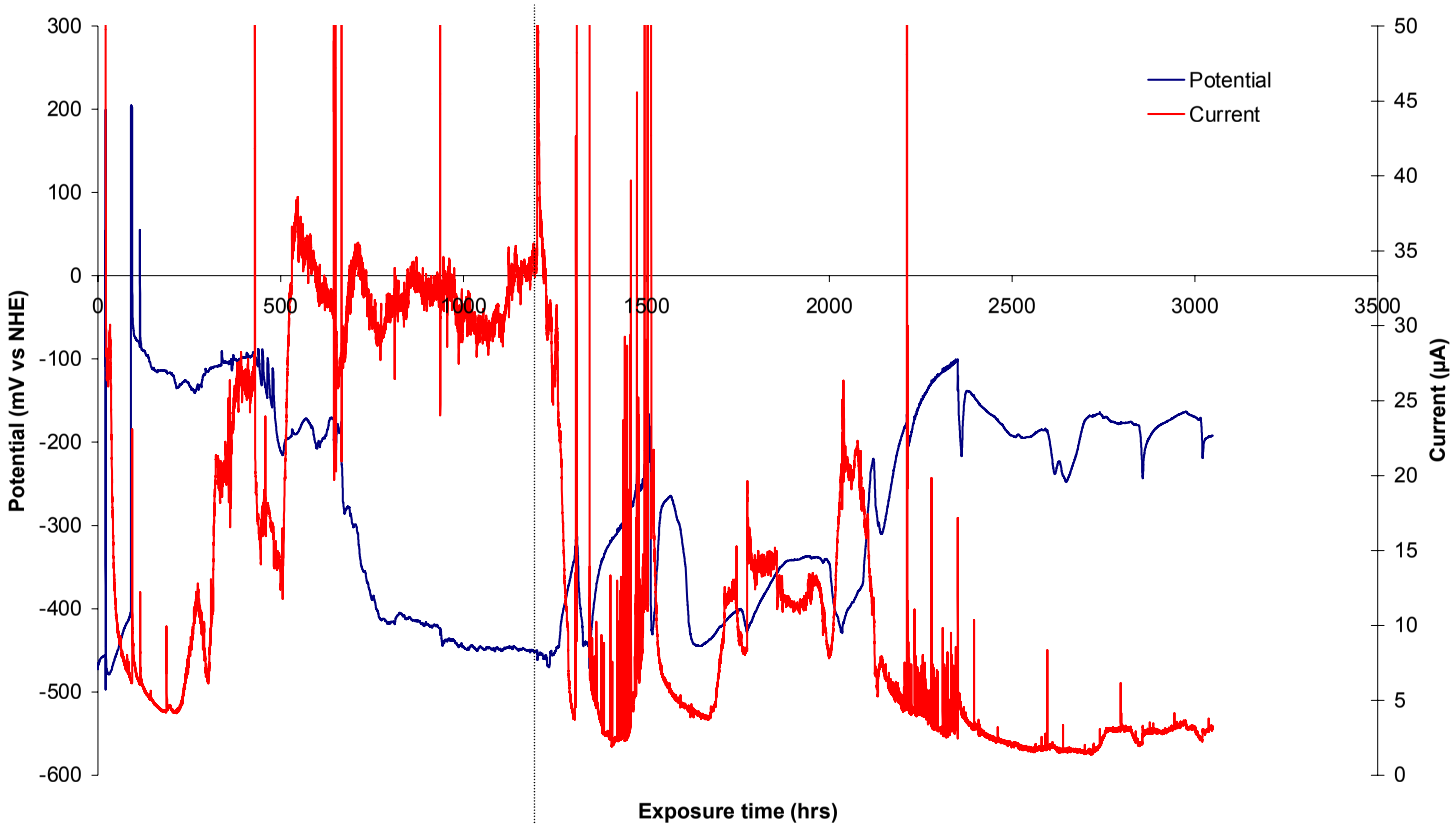

Figure 42. Currents passing between permanently coupled cast iron and copper electrodes in bentonite slurry at 50ºC - aerated initially then deaerated, and potential of coupled electrodes (Test 8, Cell B). The dotted line indicates when deaeration was commenced.

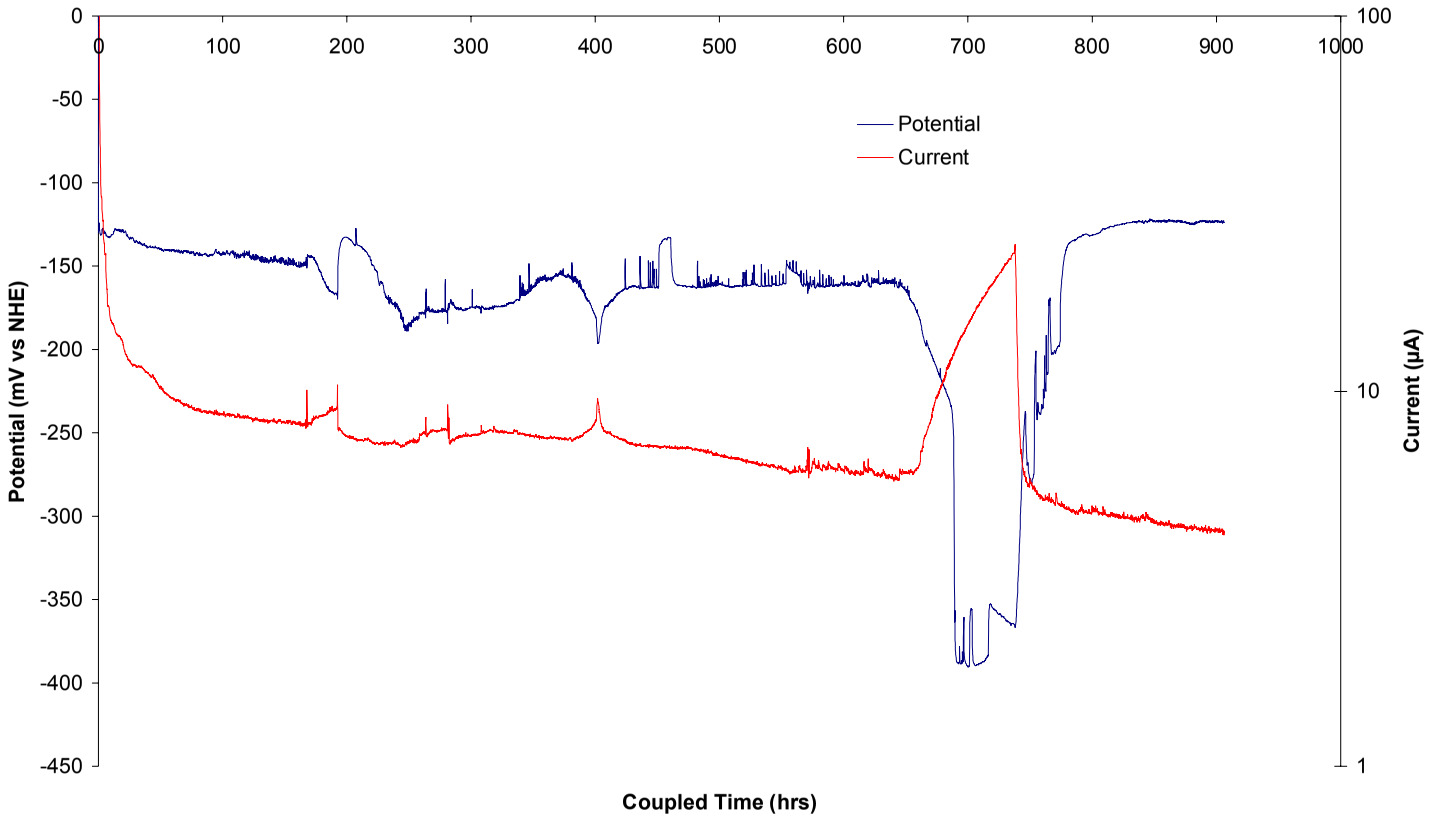

Figure 43. Currents passing between cast iron and copper electrodes in bentonite slurry at 50ºC - aerated initially then deaerated, and potential of coupled electrodes (Test 8, Cell A). The electrodes were coupled after 1064 hours exposure to solution (time after coupling shown).

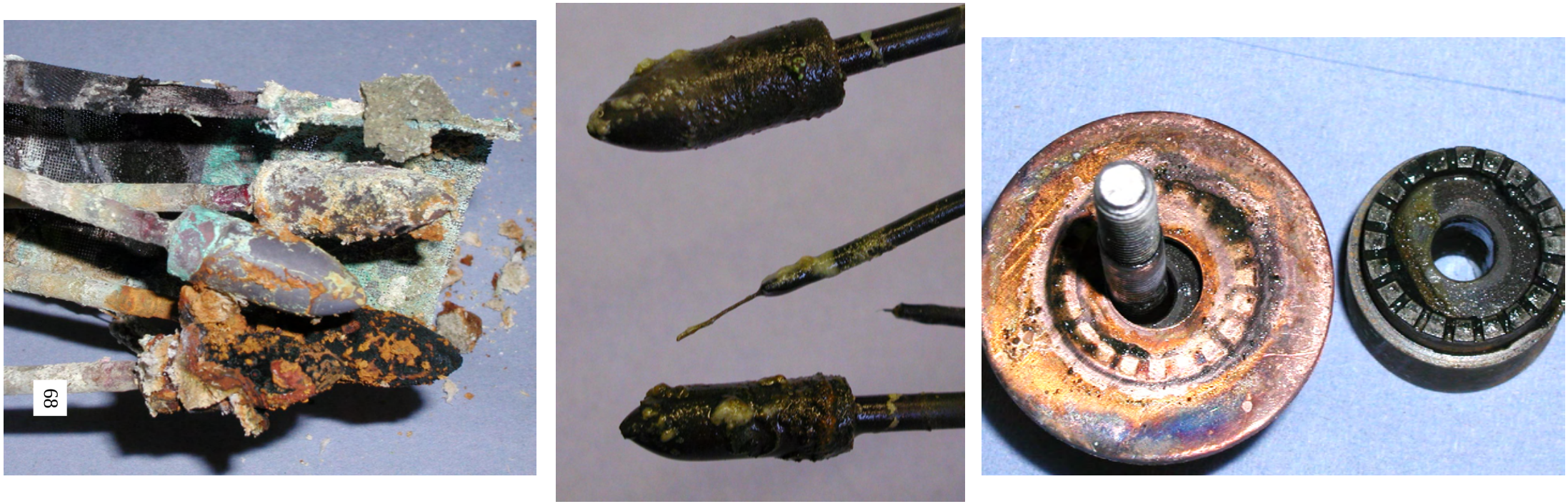

Figure 44. Specimens at end of Test 8 (bentonite slurry at 50° C- aerated initially then deaerated).

Appendices

CONTENTS

Appendix 1

Theory of galvanic couples

1. Theory of galvanic couples

There are five main factors that influence the extent to which the galvanic coupling between two metals alters their respective corrosion rates:

- The corrosion potentials of the individual metals in the surrounding electrolyte;
- The nature of the kinetics of the cathodic reactions on the coupled metals;
- The formation and dissolution of passive films;
- The ratio between the exposed surface areas of the coupled metals;
- The conductivity of the surrounding electrolyte.

1.1 The effect of corrosion potential on galvanic corrosion rate

The corrosion of a metal, M, involves its oxidation to an M^{n+} state, and can be expressed as

$$M \rightarrow M^{n+} + ne^{-} \quad (1)$$

where n represents the number of electrons released in the reaction. In an aqueous solution there must be a counter reaction occurring on the same piece of metal, but not necessarily over equal areas of metal, in which the electrons released by oxidation cause the reduction of another chemical species, e.g. water by the reaction:

$$2H_2O + 2e^{-} \rightarrow H_2 + 2OH^{-} \quad (2)$$

Electrochemical reactions in which species are oxidised and electrons produced, i.e. equation 1, are referred to as anodic reactions, whilst electrochemical reactions in which species are reduced and electrons consumed, i.e.. equation 2, are referred to as cathodic reactions.

In the absence of any complicating factors such as passivation and mass transport limitations (see sections 1.3 and 1.2.2), the kinetics of electrochemical reactions are dependent on the potential of the electrode. The rates of anodic reactions increase as the potential becomes more positive, whilst the rates of cathodic reactions increase as the potential becomes more negative. Under open-circuit conditions (i.e. the metal is not connected to any other metal or supply of current) the supply of electrons due to the corrosion of the metal (Equation 1) must be balanced by their rate of consumption (Equation 2). Therefore, the open-circuit corrosion potential (E'_{corr}) adopted by a metal must be that at which the rates of the anodic and cathodic reactions are equal. A Tafel plot (or Evans diagram) shows the interdependence of the rates of the anodic and cathodic reactions, expressed as a current, on the potential of the electrode at which the reactions occur. The intercept of the anodic and cathodic lines on the plot yields both E'_{corr} and the corrosion current density, i'_{corr}. The corrosion rate at the open-circuit is linearly proportional to the rate of the anodic reaction;

$$\text{Corrosion Rate} = \text{constant x } \frac{i'_{corr} M}{nF\rho} \quad (3)$$

where M and ρ are the molecular weight and density of the metal undergoing corrosion respectively, n is the number of electrons released by the metal to achieve its corroded state and F is Faraday's constant. The proportionality constant in equation 3 is required to convert the corrosion rate into the desired unit of time.

When two metals with differing corrosion potentials are coupled together they will be forced to adopt the same potential. This new potential will be somewhere between the two corrosion potentials of the uncoupled metals, so that the total rates of the anodic (corrosion) and cathodic reactions occurring are balanced. The corrosion rate of the metal with the more positive free corrosion potential will usually fall as it becomes the cathodic member of the couple, whereas the corrosion rate of the metal with the more negative free corrosion potential will usually increase as it becomes the anodic member of the couple. As a consequence of these shifts in potential the rates of the anodic and cathodic reactions on the individual metals will no longer be equal and instead a current will flow between them to maintain the overall balance.

Although a knowledge of the free corrosion potentials of the individual metals would allow the direction of electron flow on coupling to be determined, it provides no information on the magnitude of the current.

1.2 The effect of kinetics of the cathodic reaction in galvanic couples

In aqueous solutions the cathodic reaction that supports the corrosion process is usually the reduction of either dissolved oxygen gas or, at sufficiently negative potentials, of water itself.

1.2.1 Reduction of Water

The simplest case is when no passivation processes occur at the surface of either metal and the cathodic reaction is the reduction of water. In this case the relative catalytic activities of the two metals towards the production of hydrogen will determine the size of the galvanic current density, i_g, that flows between them. The Tafel relationship shows that for the case where the uncoupled corrosion rate of the more negative metal is much higher than the uncoupled corrosion rate of the more positive one (i.e. all the cathodic current produced at both halves of the couple can be assumed to support the corrosion of the anodic half), the galvanic current is given by [1];

$$\log i_g = \frac{-\left(E_g - 0.0591pH\right)}{\beta_c} + \log \frac{A_c}{A_a} i_{o,c} \tag{4}$$

where E_g is the corrosion potential of the galvanic couple, β_c and $i_{o,c}$ are the Tafel slope and the exchange current density respectively for the hydrogen evolution reaction at the cathode, and A_c and A_a are the exposed surface areas of the cathode and anode metals respectively. Equation 4 also assumes that no overpotential is required on either half of the couple in order to drive the water reduction reaction (i.e. no displacement from the equilibrium potential is needed in order for the water reduction reaction to proceed).

However, water reduction can take place on both halves of the galvanic couple. Therefore the corrosion current density, i_{corr}, on the more anodic half of the couple is given by the sum of the galvanic current density plus the cathodic current due to the reduction of water on its own surface;

$$\log i_{corr} = \frac{-\left(E_g - 0.0591pH\right)}{\beta_c'} + \log i_{o,c}' + \log i_g \tag{5}$$

where β'_c is the Tafel slope and $i'_{o,c}$ is the exchange current density for the hydrogen evolution reaction at the anode. In the case of a large anode and a small cathode the contribution to the total cathodic current from hydrogen evolution at the nominal anode may be greater than that from the cathode. It should be noted that under these circumstances experimental measurement of the galvanic current with a zero resistance ammeter would provide an under-estimation of the corrosion rate of the anode.

1.2.2 Reduction of Oxygen

Oxygen gas is only sparingly soluble in water (~8 ppm at STP), so the mass transport processes that replace consumed oxygen by distribution from a liquid-gas interface tend to be slow. This means that if oxygen is consumed at a metal's surface to support the corrosion reaction, it will be only slowly replaced by fresh oxygen from the bulk of the solution. As a result there is a finite limit to the cathodic current density, i_{lim}, available from the reduction of oxygen before its concentration at the surface of the metal is reduced to zero. At this point the corrosion potential of the metal must fall to a new value in order to obtain a fresh source of cathodic current, e.g. by the water reduction reaction.

When the reduction of oxygen is under mass transport control, as is usually the case, the limiting current, i_{lim}, is expected to be independent of the nature of the metal. However, in practice, metals which form corrosion products that cannot be electrochemically reduced (i.e. converted to metal) at the corrosion potential of the galvanic couple, tend to be less efficient oxygen cathodes than 'oxide free' metals [1]. This is due to the high electronic resistance of corrosion films, R_f, that either restricts the areas that can act as effective cathodes, or causes an $i_g R_f$ potential drop to develop across the film, reducing the driving force of the cathodic reaction. Bianchi et al [2] classified a range of different metals in order of decreasing efficiency, with respect to oxygen reduction:

platinum > graphite > copper > stainless steel > zirconium > aluminium.

1.2.3 Reduction of Corrosion Films

A third common source of cathodic current, along with water reduction and oxygen reduction, is the reduction of a corrosion product, usually an oxide, which may have formed prior to the electrical coupling of two metals. However, this is only a temporary process, for once all the corrosion product has been reduced a new source of cathodic current will be required [3]. The reduction of an oxide on the cathode acting as a sink for electrons can therefore be discounted under the long-term steady state conditions expected in a nuclear waste repository. Nevertheless, the presence of corrosion products on the cathode could lead to galvanic corrosion rates being over-estimated in short-term experiments.

2.3 The effect of formation and dissolution of passive films on galvanic corrosion rate

Normally when a metal undergoing active corrosion is coupled to a more noble metal, its corrosion rate increases. However, in some cases the coupling action can pull the active metal into a potential regime where the development of a passive film is thermodynamically favoured and thus its corrosion rate may actually decrease [4].

In a similar manner if the more noble metal is protected by a passive film that is reducible at the corrosion potential of the galvanic couple, its corrosion rate could increase once this film has been completely reduced [5]. In extreme cases this could lead to a reversal in the direction of flow of the galvanic current.

Polarity reversals can also be caused by changes in the lattice structure of an oxide film, leading to a change in electrical conductivity [6-8]. However, this phenomenon is usually associated with a change in the temperature of the surrounding electrolyte, rather than due to electrochemical reactions [7,9-11].

If the more negative metal is already in a passive state the coupling of a second metal will not alter its corrosion rate, unless localised corrosion is initiated or the galvanic couple moves the negative metal into the transpassive state.

1.4 The relationship between the ratio of exposed areas and the galvanic corrosion rate

In most instances where the cathodic current is supplied by the reduction of oxygen, diffusion of oxygen to the cathode metal is the rate-limiting step. Whitman and Russell [12] have shown that in this situation the galvanic current is directly proportional to the area of the cathodic metal, but independent of the area of the anodic metal. This is known as the catchment area principle. In practice this means that if cathodes of standard area are coupled to a series of anodes of varying sizes, the same galvanic current will flow across each couple. The increase in the corrosion rate of the anodic member of a couple, due to galvanic coupling, is proportional to the galvanic current divided by its exposed surface area (i.e. proportional to the galvanic current density). Therefore the increased corrosion rates of the series of anodes coupled to standard cathodes will be inversely proportional to their exposed areas (Note that this is no longer valid in solutions with a low conductivity - see section 1.5).

When the kinetics of the cathodic reaction are under purely electron transfer control, as is usually the case when the reaction is the reduction of water, equation 4 shows that the galvanic current density, i_g, depends on the corrosion potential of the galvanic couple, E_g. If the fraction of the total cathodic current produced from the cathode metal is much greater than that from the anode metal, then the dependence of the galvanic corrosion rate on the ratio of the areas of the two coupled metals is given by;

$$i_{corr} = i'_{corr}\left[\frac{i_{o,c}\,A_c\,\exp(\beta_c\eta)}{i'_{o,c}\,A_a\,\exp(\beta'_c\eta)}\right]^{\left(\frac{\beta_a}{\beta_a+\beta_c}\right)} \tag{6}$$

where i'_{corr} is the corrosion rate of the anode before coupling, β_a is the Tafel slope of the metal dissolution reaction at the anode and η is the overpotential of the cathodic reaction (assumed to be the same at both the anode and cathode).

If the exchange current densities and Tafel slopes for the cathodic reaction on the cathode and the anode are approximately the same equation 6 simplifies to;

$$i_{corr} = i'_{corr}\left[\frac{A_c}{A_a}\right]^{\left(\frac{\beta_a}{\beta_a+\beta_c}\right)} \tag{7}$$

1.5 The effect of electrolyte conductivity on the galvanic corrosion rate

The conductivity of the electrolyte surrounding a galvanic couple also affects the rate of corrosion, for the following reasons. The rate of an electrochemical reaction at the surface of a metal surface, such as corrosion, depends on the potential drop across the metal/electrolyte interface. The magnitude of this potential drop can be controlled by the application of an external potential, via a potentiostat. However, if the current collecting electrode (sometimes called the counter, secondary or auxiliary electrode) is placed near an area of the metal working electrode, the potential drop across the metal/electrolyte interface at this location, and hence the current density, will be greater than that at areas of the metal further away (iR drop effects). The extent of the difference between the potential drops across the metal/electrolyte interface in these two areas of the metals will depend on the conductivity of the surrounding electrolyte. A more detailed explanation of this effect has been provided by De Levie [13], who produced an electrochemical model for a single pore electrode, (i.e. a tube), under potentiostatic control, a system that has a surprising amount in common with galvanic couples.

Galvanically coupling two different metals together is essentially equivalent to applying a voltage at the bimetallic junction. This increases the potential drop across the electrochemical interface in the region close to the bimetallic junction. However, the resistance of the surrounding electrolyte reduces the influence of the galvanic couple at points further away. The higher the resistance of the solution the shorter the distance over which the galvanic couple can increase the potential drop across the electrochemical interface sufficiently to alter the corrosion rate.

The rate of galvanic corrosion in the close vicinity of the bimetallic junction is usually unaffected by the conductivity of the solution, since it is generally held near maximum by polarisation affects [1]. Bardal et al [14] have reported slightly higher corrosion rates in the vicinity of the bimetallic junction as the conductivity of the electrolyte was reduced.

References

1 M.J. Pryor and D.J. Astley, *Bimetallic Corrosion,* in 'Corrosion', eds. L.L. Shreir, R.A. Jarman and G.T. Burstein, Chap. 1.7, Vol. 1, 3rd Edition, Butterworth Heinemann, Oxford, 1994.

2 G. Bianchi, F. Mazza and T. Mussini, *Electrochemical Processes of Oxygen and Hydrogen Peroxide in Metal Corrosion and Protection*, 2nd International Congress for Metallic Corrosion, pp. 893-904, New York, 1963.

3 J.B. Dyess and H.A. Miley, *Tarnish Films on Copper*, Trans. Amer. Inst. Min. (Metall) Engrs. **133**, 239, 1939.

4 M.J. Pryor and D.S. Keir, *Galvanic Corrosion. I Current Flow and Polarization Characteristics of the Aluminium-Steel and Zinc-Steel Couples in Sodium Chloride Solution*, J. Electrochem. Soc. **104,** 269, 1957.

5 G.O. Davis, J. Kolts and N. Sridhar, *Polarisation Effects in Galvanic Corrosion*, Corrosion **42,** 329, 1986.

6 G. Schikorr, *The Cathodic Behaviour of Zinc Versus Iron in Hot Tap Water*, Trans. Electrochem. Soc. **76,** 247, 1939.

7 R.B. Hoxeng and C.F. Prutton, *Electrochemical Behaviour of Zinc and Steel in Aqueous Media*, Corrosion **5**, 330, 1949.

8 L. Kenworthy and M.D. Smith, *Corrosion of Galvanized Coatings and Zinc by Waters Containing Free Carbon* Dioxide, J. Inst. Met. **70,** 463, 1944.

9 G.K. Glass and V. Ashworth, *The Corrosion Behaviour of the Zinc-Mild Steel Galvanic Cell in Hot Sodium Bicarbonate* Solution, Corrosion Science **25,** 971, 1985.

10 D.R. Gabe and A.M. El Hassan, *Potential Reversals for Aluminium Alloy-Mild Steel Galvanic Couples in Simulated Natural Waters*, Br. Corr. J. **21,** 185, 1986.

11 P.T. Gilbert, *The Nature of Zinc Corrosion Products*, J. Electrochem. Soc. **99,** 16, 1952.

12 W.G. Whitman and R.P. Russell, *The Natural Water Corrosion of Steel in Contact with Copper*, Ind. Eng. Chem. **16**, 276, 1924.

13 R. De Levie in 'Advances in Electrochemistry and Electrochemical Engineering', ed. P. Delahay, **Vol. 6**, John Wiley & Sons, New York, 1967.

14 E. Bardal, R. Johnsen and P.O. Gartland, *Prediction of Galvanic Corrosion Rates and Distribution by Means of Calculation and Experimental Models*, Corrosion **40**, 628, 1984.

ISSN 1404-0344
CM Digitaltryck AB, Bromma, 2005